Neurobiology of Aging 129 (2023) 28–40

Contents lists available at ScienceDirect

Neurobiology of Aging

journal homepage: www.elsevier.com/locate/neuaging.org

Plasma neurofilament light and brain volumetric outcomes among middle-aged urban adults

May A. Beydoun [a,*,1], Nicole Noren Hooten [a], Hind A. Beydoun [b], Jordan Weiss [c], Ana I. Maldonado [a,d], Leslie I. Katzel [e,f], Christos Davatzikos [g], Rao P. Gullapalli [h], Stephen L. Seliger [i], Guray Erus [g], Michele K. Evans [a], Alan B. Zonderman [a], Shari R. Waldstein [d,e,f]

[a] Laboratory of Epidemiology and Population Sciences, NIA/NIH/IRP, Baltimore, MD, USA
[b] Department of Research Programs, Fort Belvoir Community Hospital, Fort Belvoir, VA, USA
[c] Department of Demography, University of California Berkeley, Berkeley, CA, USA
[d] Department of Psychology, University of Maryland, Baltimore County, Catonsville, MD, USA
[e] Geriatric Research Education and Clinical Center, Baltimore VA Medical Center, Baltimore, MD, USA
[f] Division of Gerontology, Geriatrics and Palliative Medicine, Department of Medicine, University of Maryland School of Medicine, Baltimore, MD, USA
[g] Artificial Intelligence in Biomedical Imaging Laboratory (AIBIL), Perelman School of Medicine, University of Pennsylvania, Philadelphia, PA, USA
[h] Department of Diagnostic Radiology and Nuclear Medicine, University of Maryland School of Medicine, Baltimore, MD, USA
[i] Division of Nephrology, Department of Medicine, University of Maryland School of Medicine, Baltimore, MD, USA

ARTICLE INFO

Article history:
Received 13 February 2023
Revised 5 April 2023
Accepted 30 April 2023
Available online 2 May 2023

Keywords:
Neurofilament light chain
Hippocampus
Brain volumes
White matter lesion
Aging

ABSTRACT

Elevated plasma neurofilament light chain (NfL) is associated with dementia though underlying mechanisms remain unknown. We examined cross-sectional relationships of time-dependent plasma NfL with selected brain structural magnetic resonance imaging (sMRI) prognostic markers of dementia. The sample was drawn from the Healthy Aging in Neighborhoods of Diversity Across the Life Span (HANDLS) study, selecting participants with complete v_1 (2004–2009) and v_2 (2009–2013) plasma NfL exposure and ancillary sMRI data at v_{scan} (2011–2015, n = 179, mean v_1 to v_{scan} time: 5.4 years). Multivariable-adjusted linear regression models were conducted, overall, by sex, and race, correcting for multiple testing with q-values. $NfL_{(v1)}$ was associated with larger WMLV (both Log_e transformed), after 5–6 years' follow-up, overall ($\beta = +2.131 \pm 0.660$, b = +0.29, $p = 0.001$, and q = 0.0029) and among females. $NfLv_2$ was linked to a 125 mm^3 lower left hippocampal volume ($p = 0.004$ and q = 0.015) in reduced models, mainly among males, as was observed for annualized longitudinal change in NfL (δNfL_{bayes}). Among African American adults, NfL_{v1} was inversely related to total, gray and white matter volumes. Plasma NfL may reflect future brain pathologies in middle-aged adults.

1. Introduction

Axonal damage in neurons can lead to the release of cytoskeletal proteins, such as neurofilaments into the extracellular space and subsequently into the cerebrospinal fluid (CSF), and then into the blood at a lower concentration (Zhao et al., 2019). Therefore, exploring the use of neurofilaments, in particular neurofilament light (NfL), as an indicator of neuroaxonal damage has become a recent focus. Importantly, blood-based markers have many advantages over using CSF and neuroimaging measures to monitor

Abbreviations: δ, annualized change; C-TRIM, Core for Translational Research in Imaging @ Maryland; FDR, false discovery rate; FLAIR, fluid-attenuated inversion recovery; FOV, field of view; GM, gray matter; HANDLS, Healthy Aging in Neighborhoods of Diversity across the Life Span study; HS, high school; ICV, intracranial volume; IRB, Institutional Review Board; MICO, multiplicative intrinsic component optimization; MP-RAGE, magnetization prepared rapid gradient echo; MRI, magnetic resonance imaging; MRV, medical research vehicle; MUSE, Multi-atlas region Segmentation utilizing Ensembles; NfL, neurofilament light; ROI, regions of interest; sMRI, structural MRI; TBV, total brain volume; US, United States; v_1, visit 1; v_2, visit 2; v_{scan}, HANDLS SCAN visit; WM, white matter; WML, white matter lesion; WMLV, white matter lesion volume; WHO, World Health Organization.

* Correspondence to: NIH Biomedical Research Center, National Institute on Aging, IRP, 251 Bayview Blvd., Suite 100, Room #: 04B118, Baltimore, MD 21224, USA.
E-mail address: baydounm@mail.nih.gov (M.A. Beydoun).

[1] MAB had full access to the data used in this article and completed all the statistical analyses.

0197-4580/
https://doi.org/10.1016/j.neurobiolaging.2023.04.013

neurodegeneration. Blood sample acquisition is noninvasive, more cost-effective, accessible to diverse clinical settings, and more feasible for time-dependent assessment. Methods measuring blood levels of NfL have recently become more sensitive (Kuhle et al., 2016), a development with a potential for large-scale applications in clinical practice and in randomized clinical trials to identify high-risk groups for all-cause and Alzheimer's disease (AD) dementia (Raket et al., 2020). The focus of much prior research has been on the association of plasma NfL with late AD (de Wolf et al., 2020), despite plasma NfL's link to frontotemporal degeneration (Scherling et al., 2014), multiple sclerosis (Teunissen et al., 2005), traumatic brain injury (Shahim et al., 2016), and other neurodegenerative diseases, including vascular dementia (Khalil et al., 2018), which rendered NfL indicative of general neuroaxonal damage and a marker for nonspecific neurodegeneration. Recent data also indicate that NfL may be a useful biomarker in the early preclinical stages of AD (Giacomucci et al., 2022).

Blood NfL is associated with neurodegenerative diseases and cerebrovascular events and diseases, being elevated in patients with ischemic stroke (Uphaus et al., 2019) and small vessel disease (Duering et al., 2018) and associated with stroke severity and white matter lesion volume (WMLV) among ischemic stroke patients, predicting adverse clinical outcomes (Egle et al., 2021; Uphaus et al., 2019). Consequently, blood NfL levels may also reflect neuroaxonal damage caused by both acute and progressive cerebrovascular events. Generally, reduced cortical and hippocampal brain volumes, and increased WMLV were linked to poor cognitive performance associated with AD (Beydoun et al., 2021a; Hsu et al., 2018; Walter et al., 2019). Recently, CSF NfL levels were positively correlated with WMLV (Jonsson et al., 2010). With NfL (in blood or CSF) capturing subcortical large-caliber axonal degeneration (Norgren et al., 2003), plasma NfL concentrations strongly correlate with corresponding CSF NfL concentrations (Raket et al., 2020), adding to NfL's clinical utility for monitoring both neurocognitive and cerebrovascular diseases.

Plasma NfL's association with brain aging's neuroimaging measures (He et al., 2020; Khalil et al., 2020; Merluzzi et al., 2019; Mielke et al., 2019; Nyberg et al., 2020; Peters et al., 2020; Rajan et al., 2020; Rubsamen et al., 2021) has been tested without evaluating racial and gender group differentials. Associations of plasma NfL measured at different time points with follow-up brain volumetric markers of subclinical brain pathology prognostic of future stroke and dementia among healthy middle-aged adults are largely unknown. Thus, our study (i) examined baseline plasma NfL's association with follow-up brain volumetric outcomes, including global, cortical gray matter (GM) and white matter (WM), hippocampal, and WMLVs; (ii) examined NfL at follow-up in relation to these brain volumetric outcomes at follow-up; (iii) examined annualized change in NfL and "tracking high" and "tracking low" NfL longitudinal exposures in relation to these brain volumetric outcomes at follow-up; and (iv) tested sex and race as putative effect modifiers in these associations.

2. Methods

2.1. Study design

The Healthy Aging in Neighborhoods of Diversity across the Life Span (HANDLS) study includes a sociodemographically diverse sample of middle-aged White and African American urban adults selected using an area probability strategy (Age_{v1}: 30–64 years, Baltimore, MD, USA) (Evans et al., 2010). HANDLS, an ongoing prospective cohort study initiated by the National Institute on Aging in 2004 (Evans et al., 2010), included interviews among identified participants through random sampling of addresses within each census tract, with eligibility criteria listed elsewhere (Evans et al., 2010).

The initial recruitment and examination were composed of two phases, with Phase 1 including a dietary interview and several demographic and psychosocial scales elicited from participants within their homes. Phase 2 examined participants in medical research vehicles (MRVs) parked in close proximity to their neighborhoods (Evans et al., 2010). MRV exams elicited a second dietary interview from participants and included other physical, psychosocial, and medical assessments, personal and family health history, neuropsychological tests, physical performance by a brief screening battery, physical examination by a physician, and inventories to assess depressive symptoms (Evans et al., 2010). Eight hours or longer of fasting was required prior to MRV visits, where plasma specimens were collected, aliquoted, and frozen at −80 °C. Phases 1 and 2 data are labeled as visit 1 (v_1, 2004–2009). Comparable follow-up MRV visits were conducted, including at visit 2 (v_2, 2009–2013). For our present study, only visit one covariate, including biochemical and hematological indices, was selected for our analyses.

In our present study, we included participants with complete and valid sMRI data at the HANDLS SCAN visit and complete NfL data at v_1 and v_2 (Fig. 1). HANDLS SCAN recruited participants from consecutive waves of first and second follow-up examinations (2011–2015). Participants excluded from the HANDLS SCAN examination had self-reported histories of HIV, neurological and/or terminal diseases, stroke, transient ischemic attack, or carotid endarterectomy or had specific MRI contraindications (e.g., indwelling ferromagnetics). The sample recruited into HANDLS SCAN represented the overall HANDLS study sample in educational attainment, poverty status, and sex ($p > 0.05$) but had more White and younger participants ($p < 0.05$).

Here, we analyzed plasma NfL data from visits 1 (v_1: 2004–2009) and 2 (v_2:2009–2013) in relation to follow-up data measured in a subsample of N_{max} = 238 participants within the HANDLS SCAN substudy (v_{scan}: 2011–2015) (Waldstein et al., 2017). Thus, this was a cross-sectional analysis with outcomes measured at one time point and exposures measured as part of the MRV visits (v_1 or v_2); outcomes were MRI assessments obtained from v_{scan} reflecting brain volume and WMLV (Waldstein et al., 2017). The mean ± SD follow-up time between v_1 and v_{scan} was 5.61 y ± 1.90.

Of the initial 3720 participants, two subsamples were identified from v_1 (n = 694) and v_2 (n = 709) (Fig. 1). These subsamples were used for the LASSO covariate selection process (see Supplemental Method 4), further restricting to participants with complete data on NfL at both visits 1 and 2, and more importantly to the HANDLS SCAN substudy participants with complete sMRI data (n = 238), yielding a final sample of 179 participants with complete brain sMRI and NfL (v_1 and v_2) data. This final sample (N = 179), compared with the remaining excluded participants from the initial n = 3720, had higher proportions of White adults (59% vs. 40%, $p < 0.05$) and individuals living above poverty (69% vs. 58%, $p < 0.05$). Moreover, we conducted a sensitivity analysis, whereby we excluded individuals with a history of head injuries and with a total Mini-Mental State Exam (Folstein et al., 1975) v_1 score < 23, yielding n = 147 with normal cognition and free from head injuries.

Written informed consent was provided by all participants. HANDLS and HANDLS-SCAN study protocols were approved by the National Institute on Environmental Health Sciences Institutional Review Board (IRB) of the National Institutes of Health. Furthermore, HANDLS-SCAN was approved by the IRBs of the University of Maryland School of Medicine and the University of Maryland, Baltimore County.

2.2. Brain sMRI: Volumetric outcomes

Cranial MRI assessments were conducted on a Siemens Tim-Trio 3.0 Tesla unit scanner. We used magnetization-prepared rapid gradient

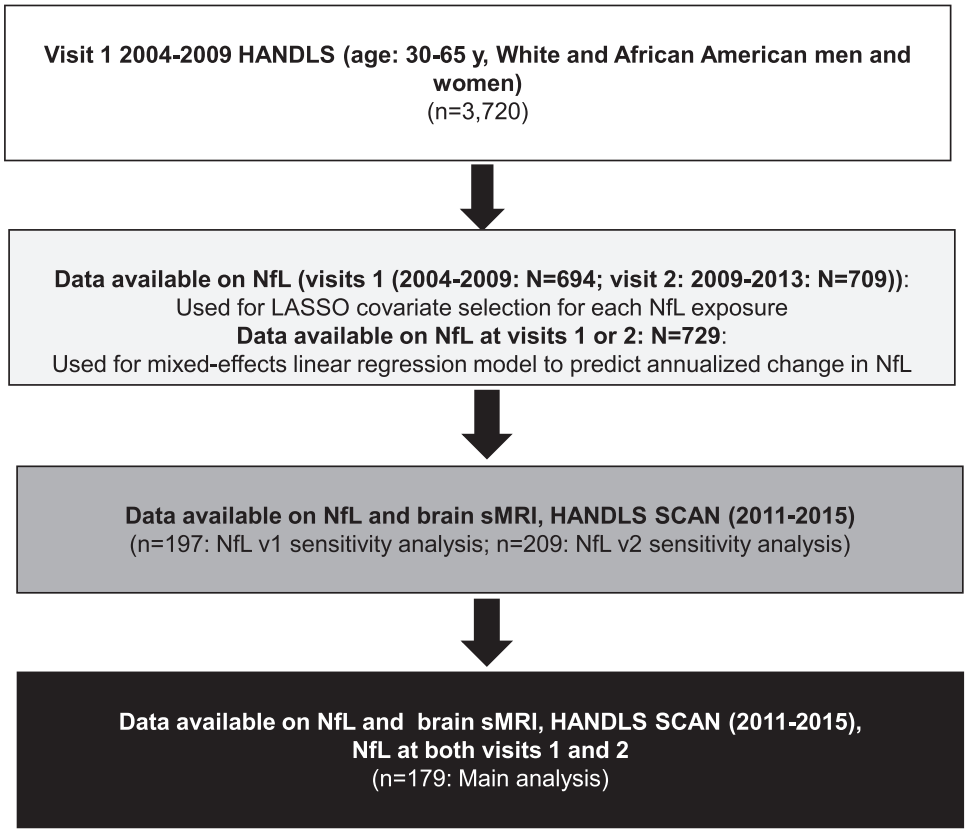

Fig. 1. Study participant schematic: HANDLS 2004–2013 and HANDLS-SCAN 2011–2015 (Visit 1 refers to HANDLS 2004–2009; Visit 2 refers to HANDLS 2009–2013; and HANDLS-SCAN visit (v_{scan}) was carried out between 2011 and 2015). Abbreviations: HANDLS, Healthy Aging in Neighborhoods of Diversity Across the Life Span.

echo (MP-RAGE) to perform volumetric measurements for anatomical regions, and volumetric measures were estimated per region of interest (ROI). Supplemental method 1 details methods used to estimate ROI-specific volumes and quality assurance. A multimodal lesion segmentation technique was used based on supervised learning, which utilizes a model trained on manually segmented lesions and then applies them to segment ischemic lesions (Lao et al., 2008). The method relies on coregistering T1, T2, FLAIR, and PD scans, histogram normalization to a template image, extraction of features, voxelwise label assignment, and elimination of false positives. We applied a novel multiatlas label fusion methodology to segment the brain into anatomical ROIs (Doshi et al., 2013). We computed volumetric measurements for normal and abnormal (with lesion) tissue within each ROI and then grouped those into larger anatomical regions using a hierarchical representation. Specifically, WM lesions were identified by segmenting hyperintensities on FLAIR images. We used an automated multimodal segmentation method that uses supervised learning. The method was trained on an external training set with FLAIR and T1-weighted MRI images and voxelwise ground-truth WM lesion labels. We segmented the T1-weighted image of each subject into 145 ROIs using a multiatlas label fusion method (Doshi et al., 2016). These ROIs were also used for calculating larger derived ROIs in multiple resolution levels, including total GM and total WM, using a predefined ROI hierarchy. ROI labels for each subject were used to calculate regional volumes of different tissue types and regional volumes of abnormal tissues, specifically regional WM lesions in this present study.

The current study focused on hippocampal volumes [Left(L) and Right(R)] and overall WMLV (Log_e transformed) as primary outcomes while also examining total brain volume (TBV), GM and WM volume, and ROI-specific WMLV (cubic root transformed), as secondary outcomes of interest. In addition, regional volumes within GM and WM, taking laterality into account, were also examined as a post hoc analysis (i.e., L/R, regional WM and GM for "frontal," "temporal," "parietal," and "occipital" regions). However, this analysis was only presented if GM and/or WM showed a significant association with each of the two main exposures, namely, v_1 or v_2 NfL. All analyses with lesion volume and small ROIs (e.g., hippocampal volumes or ROI-specific WMLV) were adjusted for intracranial volume (ICV).

2.3. NfL at v_1 and v_2

After an overnight fast, MRV visit blood samples were collected (9:30 AM through 11:30 AM) into EDTA blood collection tubes, which were centrifuged at 600 *g* for 15 min, with the buffy coat removed. These latter steps were repeated twice while visually inspecting for hemolysis. Upon aliquoting, plasma samples were stored at −80 °C. Plasma NfL concentrations were quantified using the Simoa NF-light Advantage Kit (Quanterix, Billerica, MA, USA), after following kit instructions. Samples from distinct visits were run on one plate for each individual, and plates were balanced for all individuals within each demographic stratum (race/sex/poverty). After the 4-fold dilution of plasma samples, concentrations were adjusted for dilution correction. Pooled plasma samples from two individuals were run in duplicate on all plates and the average intra-assay and inter-assay coefficient of variations were 4.5% and 7%, respectively. Information on limits of detection and quantification for the runs of this specific assay has been described previously (Beydoun et al., 2021b). Plasma NfL was assessed with ≤2 repeats/participant at v_1 and/or v_2. The NfL_{v1} and NfL_{v2} exposures are detailed in supplemental Method 2. NfL_{v1} is the baseline NfL measured at v_1 (2004–2009), while NfL_{v2} was measured

at the first follow-up visit v_2 (2009–2013). Both of these observed measurements are exposures of interest in the present study. A secondary exposure of interest is "tracking high" or "tracking low" of NfL over time, defined by a common median level of untransformed plasma NfL. These 2 exposures are binary with 1 = tracking high/low between the 2 visits (i.e., greater than median at both visits for "tracking high" and less than or equal to median value for "tracking low"); 0 = otherwise. This analysis is only presented for selected outcomes, whereby at least 1 of 2 previous exposures is found to be significantly associated with those outcomes of interest, thus enhancing the interpretation of visit-specific findings. We also report the δNfL as the annualized rate of change between $NfLv_1$ and $NfLv_2$ measurements (Beydoun et al., 2021b) for descriptive purposes (see Supplemental Method 3).

2.4. Covariates

In all models, exposure-outcome associations were adjusted for v_1 age (years), sex (male = 1, female = 0: primary stratifying variable), self-identified race (African American = 1, White = 0), self-reported household income either < 125% = 1 or ≥125% = 0 of the 2004 Health and Human Services poverty guidelines (termed poverty status) (Nilsson et al., 2019), and time (days) between v_1 MRV visit and v_{scan}. Models also included ICV for select volumetric outcomes, namely, hippocampal volume (L/R), total and small ROI-specific lesion volumes, and small ROI-specific brain volumes. All models were further stratified by sex (main potential effect modifier) and race (secondary potential effect modifier). Additional covariates were added to models after screening for their associations with NfL exposures using machine learning techniques (online Supplemental Method 4). Those are considered explanatory pathways by which main exposures may be linked with outcomes of interest.

2.5. Statistical analyses

We used Stata version 16.0 (STATA, 2019) for all analyses. We computed means and proportions of sample characteristics and tested for sex differences using Student's t and χ^2 tests as appropriate. Regression modeling (linear and multinomial logit) was used in order to assess sex differences in various measures, including exposures, outcomes, and covariates, after adjustment for race, poverty status, and age in one model, and additional adjustment for ICV in a second model. We further described the sample characteristics by tertiles of NfL_{v1} and NfL_{v2} (Supplementary Table 1).

To test the main hypotheses, a series of multivariable regression models were then estimated with sequential covariate adjustment, using the complete sample with further sex stratification, wherein each of two exposures was added as potential predictors for each sMRI outcome measured at v_{scan}. For every model, we obtained estimates of standardized b that we interpreted as a 1 SD change in sMRI outcome per 1 SD change in the specified continuous exposure (i.e., NfL at v_1 and v_2). We decided a priori to classify standardized b estimates > 0.20 as moderate-to-strong and estimates between 0.10 and 0.20 as weak-to-moderate. In another set of secondary models, we considered the annualized rate of change in NfL (Log_e transformed) as a main exposure while adjusting for NfL at v_1, Log_e transformed along with other potentially confounding covariates, using a similar modeling strategy.

We conducted our analysis in four stages. Our first analysis (*Analysis A*) included measures of total brain, total WM, and total GM volumes. Our second analysis (*Analysis A′*) was a post hoc regional analysis for *Analysis A* that detailed cortical volumes within GM and WM (i.e., as L/R, GM/WM, frontal, temporal, parietal, and occipital); this yielded 16 post hoc outcomes. Results from *Analysis A′* were presented only if, for a given model, at least one *Analysis A* exposure-outcome association was statistically significant ($p_{uncorr} < 0.05$) in a given sample. In *Analysis B,* we examined L/R hippocampal volumes as our primary outcomes. In *Analysis C*, total WM lesion volume (Log_e transformed) was our outcome of interest. If at least one model showed significant findings for exposure-outcome association at type I error of 0.05, another analysis was conducted examining small ROI-specific associations (*Analysis C′*). For each stage, we considered models with minimal covariate adjustment as our primary analyses to test the hypotheses of interest. The post hoc analysis (*Analyses A′* and *C′*) and subsequent models with sequential covariate adjustment were considered secondary analyses, as were race-specific analyses conducted for *Analyses A* and *C*.

Secondary outcomes were WMLV at each independent ROI (Supplemental Table 1**,** 61 WM-related ROIs with a nonzero WMLV). These selected regional WMLVs were cubic-root transformed, and the resulting values were then transformed into standardized z-scores. In addition, of the 61 WM-related ROIs, only 24 were selected having > 5% with nonzero WMLV on the untransformed scale. A sensitivity analysis was conducted on the untransformed regional WMLVs for comparative purposes. We utilized volcano plots as a visualization tool for these select findings from ROI-specific models, focusing on **Model 1** minimally adjusted model, corrected for ICV (R Foundation for Statistical Computing, 2013). These plots display Log_{10} (p values) for each set of models, with exposures being alternatively NfL at v_1 or NfL at v_2, against standardized beta coefficients (b) on the X-axis, highlighting findings with larger b. The volcano plots visualize ROIs in terms of uncorrected p value < 0.05 showing different colors depending on whether effect size b > 0.20. Visualization of ROI-specific b with standard brain images was carried out using FSLeyes software (Jenkinson et al., 2002; Jenkinson and Smith, 2001) applied to these sMRI results for ROI-specific lesion volumes (URL: https://fsl.fmrib.ox.ac.uk/fsl/fslwiki/FSLeyes).

Type I error was set at 0.05 for uncorrected p values. We corrected for multiple testing using the false discovery rate (FDR, q-value). Each stage of analysis conducted for the overall and stratified samples was treated as separate hypotheses (i.e., *Analyses A–C*: overall versus stratified by sex). In doing so, we adjusted for multiplicity within analysis and across strata. We used this correction specifically for the model with minimal covariate adjustment (i.e., Model 1) for each of *Analyses A–C*. We reported FDR q-values when $P_{uncorr} < 0.05$ for exposure-outcome associations. Statistical significance in Model 1 was determined when FDR q-value < 0.05, while a q-value < 0.10 but ≥0.05 suggested a trend. Our models with sequential covariate adjustment (Models 2–6) were presented as secondary analyses designed to test mediating pathways between exposures and outcomes of interest (online Supplemental Method 4). Another sensitivity analysis was conducted in the subsample that was free from head injuries and was considered as having a normal cognitive performance at v1 based on the MMSE total score (n = 163).

3. Results

The main characteristics of the study sample are presented in Table 1, overall and stratified by sex. The total selected sample consisted of 80 males and 99 females (N = 179), with mean ± SD age of 48.3 ± 9.4 years, of whom 41.3% were African American adults and 68.7% living above poverty. Lengths of follow-up were comparable across sex. No sex differences were detected for poverty status, age, and race, nor in the NfL exposure distributions or the annualized change in NfL between v_1 and v_2. In contrast, males (vs. females) had higher odds of prediabetes, significantly higher urinary specific gravity, serum uric acid and serum creatinine levels, and serum albumin. Larger brain volumes were found among males, with the exception of hippocampal volume as % of ICV, which was higher among females. No sex differences were detected in WMLV.

Table 1
Study sample characteristics of eligible study sample by sex; HANDLS (v_1: 2004–2009; v_2: 2009–2013) and HANDLS-SCAN 2011–2015[a]

	Total (N = 179)	Females (N = 99)	Males (N = 80)	P_{sex}
Sociodemographic, lifestyle and health-related factors at v_1				
	%, Mean ± SD	%, Mean ± SE	%, Mean ± SE	
Sex, % males	44.7	—	—	
Age_{v1}	48.3 ± 9.4	47.4 ± 0.95	48.2 ± 0.98	0.59
Race, % African American	41.3	40.4	42.5	0.77[b]
% above poverty	68.7	63.6	75.0	0.10
Time between v_1 and v_{scan} (y)	5.42 ± 1.73	5.46 ± 0.18	5.36 ± 0.19	0.70
Time between v_2 and v_{scan} (y)	1.13 ± 1.21	1.17 ± 0.12	1.07 ± 0.14	0.59
Imputed covariates, % or Mean ± SE				
Body mass index, $kg.m^{-2}$	29.3 ± 0.5	30.2 ± 0.7	28.3 ± 0.6	0.047
Diabetes				
No	71.6	78.8	62.8	—
Prediabetes	17.7	11.1	25.8	0.011
Diabetes	10.7	10.1	11.4	0.47
Plasma glucose, mg/dL	99.9 ± 2.1	96.5 ± 2.2	104.1 ± 3.8	0.073
Creatinine, mg/dL	0.89 ± 0.02	0.79 ± 0.02	1.01 ± 0.03	< 0.001
Urine Specific Gravity	1.0193 ± 0.0004	1.0183 ± 0.0006	1.02047 ± 0.0007	0.025
Blood urea nitrogen, mg/dL	13.75 ± 0.31	13.33 ± 0.40	14.27 ± 0.50	0.14
Alkaline Phosphatase, U/L	75.2 ± 1.6	77.9 ± 2.2	71.9 ± 2.2	0.059
Uric acid, mg/dL	5.50 ± 0.11	4.98 ± 0.14	6.13 ± 0.15	< 0.001
Albumin, g/dL	4.34 ± 0.02	4.28 ± 0.03	4.42 ± 0.03	0.001
Eosinophils, %	2.75 ± 0.15	2.54 ± 0.21	3.00 ± 0.20	0.12
25-hydroxyvitamin D, ng/mL	22.3 ± 0.8	21.9 ± 1.25	23.0 ± 1.2	0.58
Current drug use, % yes	20.1	21.8	18.0	0.55
Self-rated health, %				
Poor/fair	21.8	25.3	17.5	—
Good	36.9	37.4	36.3	0.42
Very good/excellent	41.3	37.4	46.3	0.15
	%, Mean ± SD	%, Mean ± SE	%, Mean ± SE	
NfL, Log_e transformed (v_1)				
Mean ± SD	2.01 ± 0.53	1.97 ± 0.05	2.06 ± 0.06	0.28
Median	1.97	1.97	1.98	
IQR	1.68;2.26	1.62;2.27	1.74;2.25	
NfL, Log_e transformed (v_2)				
Mean ± SD	+2.22 ± 0.58	+2.15 ± 0.054	+2.30 ± 0.07	0.091
Median	+2.18	+2.12	+2.19	
IQR	+1.84; 2.56	1.78; 2.55	+1.94; +2.56	
δNfL, observed, annualized (Empirical Bayes)				
Mean ± SD	+0.038 ± 0.074	+0.033 ± 0.057	+0.044 ± 0.92	0.32
"Tracking high" v_1 through v_2: NfL > 8 pg/mL	36.3	35.4	37.5	0.77
"Tracking low" v_1 through v_2: NfL ≤ 8 pg/mL	36.3	37.4	35.0	0.74
sMRI measures, mm^3	*(N = 179)*	*(N = 99)*	*(N = 80)*	
Global brain volumes	**Mean ± SD**	**Mean ± SE**	**Mean ± SE**	
Total brain volume	1,142,888 ± 118,106	1,082,462 ± 8173	1,217,666 ± 12,741	< 0.001-
Gray matter	642,412 ± 65,224	611,599 ± 4794	680,543 ± 7160	< 0.001
White matter	457,267 ± 52,875	432,087 ± 3779	488,427 ± 5882	< 0.001-
Regional cortical brain volumes	**Mean ± SD**	**Mean ± SE**	**Mean ± SE**	
Left brain				
Frontal GM	93,214 ± 10,104	89,163 ± 802	98,228 ± 1145	< 0.001
Frontal WM	85,326 ± 10,333	80,698 ± 760	91,053 ± 1171	< 0.001-
Temporal GM	50,289 ± 6140	47,233 ± 427	54,072 ± 674	< 0.001[c]
Temporal WM	49,913 ± 6054	46,476 ± 431	52,942 ± 689	< 0.001
Parietal GM	46,149 ± 5674	44,208 ± 466	48,552 ± 664	< 0.001-
Parietal WM	43,897 ± 5610	41,365 ± 419	47,030 ± 626	< 0.001-
Occipital GM	38,075 ± 5221	36.164 ± 437	40,440 ± 588	< 0.001
Occipital WM	21,028 ± 2957	19,757 ± 232	22,600 ± 327	< 0.001
Right brain				
Frontal GM	93,300 ± 10,316	88,900 ± 790	98,744 ± 1166	< 0.001
Frontal WM	87,552 ± 10,687	82,820 ± 783	93,407 ± 1221	< 0.001
Temporal GM	50,289 ± 6140	48,266 ± 438	54,878 ± 644	< 0.001
Temporal WM	49,913 ± 6054	47,041 ± 429	53,465 ± 679	< 0.001
Parietal GM	46,149 ± 5674	44,654 ± 470	49,395 ± 660	< 0.001
Parietal WM	41,683 ± 5452	39,211 ± 407	44,743 ± 607	< 0.001
Occipital GM	39,335 ± 5402	36,957 ± 409	42,277 ± 605	< 0.001
Occipital WM	20,816 ± 2931	19,512 ± 236	22,429 ± 311	< 0.001
Hippocampal volume	**Mean ± SD**	**Mean ± SE**	**Mean ± SE**	
Hippocampus, Left	3537 ± 386	3414 ± 29	3688 ± 48	< 0.001
Hippocampus, Right	3827 ± 413	3706 ± 34	3978 ± 50	< 0.001
White matter lesion volume, Log_e transformed	**Mean ± SD**	**Mean ± SE**	**Mean ± SE**	
	5.65 ± 3.84	5.30 ± 0.44	6.08 ± 0.34	0.18

(*continued on next page*)

Table 1 (*continued*)

	Total (N = 179)	Females (N = 99)	Males (N = 80)	P_{sex}
Hippocampal volumes, % of intracranial volume				
Hippocampus, Left	0.265 ± 0.024	0.272 ± 0.002	0.257 ± 0.003	< 0.001
Hippocampus, Right	0.286 ± 0.025	0.295 ± 0.002	0.277 ± 0.003	< 0.001
Intracranial volume, mm³	**Mean ± SD**	**Mean ± SE**	**Mean ± SE**	
	1,339,313 ± 142,093	1,259,338 ± 9661	1,438,281 ± 14,184	< 0.001

Key: Age_{v1}, age measured at HANDLS visit 1 (2004–2009); GM, gray matter; HANDLS, Healthy Aging in Neighborhoods of Diversity Across the Life Span; HANDLS-SCAN, brain magnetic resonance imaging scan ancillary study of HANDLS; IQR, interquartile range (25th–75th percentile); IQR, interquartile range; NfL, neurofilament light; sMRI, structural magnetic resonance imaging; v_1, visit 1 of HANDLS (2004–2009); v2, visit 2 of HANDLS (2009–2013); v_{scan}, HANDLS-SCAN visit (2011–2015); WM, white matter; WRAT-3, Wide Range Achievement Test, 3rd version.

[a] Values are Mean ± SD for totals and Mean ± SE for stratum-specific or % (except for imputed data where it was Mean ± SE for totals). Volumes are expressed in mm^3. p_{sex} was obtained from nd *t*-tests for the unimputed covariates and from multinomial logit and linear regression models for the imputed data. Additional models with sex, race, age, and poverty status were conducted to test whether the sex differences were independent of other sociodemographic factors. All statistically significant sex differences at type I error of 0.05 retained their statistical significance after further adjustment for age, race, and poverty status.

[b] $p < 0.05$ for the null hypothesis that mean or proportion is equal between males and females after further adjustment for ICV.

[c] Direction of difference between males and females reverse upon further adjustment for ICV.

Upon adjustment for age, race, and poverty status, none of the statistically significant sex differences was markedly attenuated. Upon further adjustment of ICV, however, sex differences were reversed for WM volumes, whereby accounting for ICV women had larger total WM volume, and results became largely null for total GM volume. Table S2 findings are summarized in Online Supplemental Result 1.

Tables 2–3 and S3–S4 tested whether NfL measured at v_1 (Table 1) or v_2 (Table 3) was associated with neuroimaging markers of brain aging. The data were examined in both the overall sample and stratified by sex. Upon correction for multiple testing ($q < 0.05$) in minimally adjusted models that were corrected for ICV in analyses B and C, $NfL_{(v1)}$ had a moderately strong association with larger WMLV at follow-up v_{scan} visit, after a period of 5–6 years of follow-

Table 2
Minimally and BMI-adjusted associations from *Analyses A* (global, GM and WM volumes), *A′* (regional cortical GM/WM), *B* (hippocampal volume), and *C* (white matter lesion volume) versus visit 1 NfL, Log_e transformed, or NfL_{v1} (overall and stratified by sex): ordinary least square analyses; HANDLS 2004–2009 and HANDLS-SCAN 2011–2015[a]

	Model 1: Minimally adjusted					Model 2: BMI-adjusted, sensitivity analysis (SA)[b]			
	β1	(SE1)	b1	P1	q-value1	β2	(SE2)	P2	Interaction by sex
Total sample (N = 179)									
sMRI, Analysis A									
Total brain	−1042	(15,863)	−0.005	0.95	—	+1841	(16,514)	0.91	0.59
GM	−5763	(8503)	−0.046	0.50	—	−3707	(8844)	0.68	0.23
WM	+2207	(7725)	+0.022	0.76	—	+2987	(8048)	0.71	0.76
sMRI, Analysis B									
Hippocampus, Left	−49.3	(52.1)	-0.067	0.35	—	−39.9	(54.2)	0.46	0.24
Hippocampus, Right	−39.4	(53.8)	-0.050	0.47	—	−28.4	(56.0)	0.61	0.31
Analysis C									
White matter lesion volume, **Log_e transformed**	+2.131	(0.660)	+0.29	0.001	0.0029	+2.376	(0.685)	0.001	0.007
Males (N = 80)									
sMRI, Analysis A									
Total brain	−7470	(24,369)	-0.036	0.76	—	−6446	(24,763)	0.80	—
GM	−11,061	(12,684)	-0.096	0.39	—	−10,057	(12,870)	0.44	—
WM	−1460	(11,879)	-0.015	0.90	—	−1653	(12,078)	0.89	—
sMRI, Analysis B									
Hippocampus, Left	−92.6	(76.1)	-0.12	0.23	—	−85.3	(77.1)	0.27	—
Hippocampus, Right	−63.4	(78.3)	-0.08	0.42	—	−48.6	(78.7)	0.54	—
Analysis C									
White matter lesion volume, **Log_e transformed**	+1.48	(0.71)	+0.27	0.040	0.080	+1.44	(0.72)	0.049	—
Females (N = 99)									
sMRI, Analysis A									
Total brain	+7503	(20,835)	+0.046	0.72	—	+17,727	(22,535)	0.43	—
GM	+938	(11,624)	+0.010	0.94	—	+7992	(12,522)	0.53	—
WM	+8132	(10,113)	+0.109	0.42	—	+12,452	(10,958)	0.26	—
sMRI, Analysis B									
Hippocampus, Left	+56.8	(70.0)	+0.097	0.42	—	+82.6	(76.2)	0.28	—
Hippocampus, Right	+28.7	(75.5)	+0.043	0.70	—	+36.8	(82.5)	0.66	—
sMRI, Analysis C									
White matter lesion volume, **Log_e transformed**	+2.896	(1.146)	+0.332	0.013	0.053	+4.005	(1.217)	0.001	—

Key: Age_{v1}, age measured at HANDLS visit 1 (2004–2009); FDR, false discovery rate; GM, gray matter; HANDLS, Healthy Aging in Neighborhoods of Diversity Across the Life Span; HANDLS-SCAN, brain magnetic resonance imaging scan ancillary study of HANDLS; NfL, neurofilament light; SE, standard error; sMRI, structural magnetic resonance imaging; v_1, visit 1 of HANDLS (2004–2009); v_2, visit 2 of HANDLS (2009–2013); v_{scan}, HANDLS-SCAN visit (2011–2015); WM, white matter.

[a] Values are adjusted linear regression coefficients β with associated SE, standardized beta, uncorrected *p* values, corrected q-values (false discovery rate), and results of sensitivity analysis. (N) is the sample size in each analysis. Standardized betas for NfL are computed as SD in outcome per SD in visit 1 NfL and Log_e transformed. Q-values are presented only for uncorrected *p* values < 0.05 for model 1. Model 1 was adjusted for Age_{v1}, sex, race, poverty status, intracranial volume (*Analyses B* and *C*), and time of follow-up between visit 1 and v_{scan}. Volumes are expressed in mm^3.

[b] Model 2 is a sensitivity analysis further adjusting Model 1 for BMI after screening using machine learning techniques (See Supplemental methods 2).

Table 3
Minimally-adjusted and BMI-adjusted associations from analyses *A* (global GM and WM volumes), *A′* (regional cortical GM/WM), *B* (hippocampal volume) and *C* (white matter lesion volume) versus visit 2 NfL, Log_e transformed or NfL_{v2} (overall and stratified by sex): ordinary least square analyses; HANDLS 2009–2013 and HANDLS-SCAN 2011–2015[a]

	Model 1: Minimally adjusted					Model 2: BMI-adjusted, sensitivity analysis (SA)[b]			
	β1	(SE1)	b1	*p*1	q-value1	β2	(SE2)	*p*2	Interaction by sex
Total sample (N=179)									
sMRI, Analysis A									
Total brain	−3967	(13,209)	−0.02	0.76	—	−3050	(13,320)	0.82	0.38
GM	−5622	(7,078)	−0.05	0.43	—	-4874	(7128)	0.50	0.30
WM	−1217	(6,435)	−0.01	0.85	—	-1036	(6495)	0.87	0.37
sMRI, Analysis B									
Hippocampus, Left	−125.0	(42.4)	−0.19	0.004	0.015	−122.2	(42.8)	0.005	0.14
Hippocampus, Right	−100.4	(44.2)	−0.14	0.024	0.049	−97.1	(44.6)	0.031	0.14
Analysis C									
White matter lesion volume, **Log_e transformed**	+0.466	(0.565)	+0.07	0.41	—	+0.496	(0.570)	0.39	0.015
Males (N=80)									
sMRI, Analysis A									
Total brain	−15,556	(20,664)	−0.08	0.45	—	−16,032	(20,821)	0.44	—
GM	−10,368	(10,778)	−0.10	0.34	—	−10,844	(10,831)	0.32	—
WM	−7681	(10,067)	−0.09	0.45	—	−7650	(10,154)	0.45	—
sMRI, Analysis B									
Hippocampus, Left	−145.4	(63.1)	−0.21	0.024	0.19	−149.4	(63.2)	0.021	—
Hippocampus, Right	−120.9	(65.5)	−0.17	0.069	—	−127.4	(64.9)	0.054	—
Analysis C									
White matter lesion volume, **Log_e transformed**	−0.276	(0.619)	-0.06	0.66	—	-0.250	(0.622)	0.69	—
Females (N=99)									
sMRI, Analysis A									
Total brain	+7559	(18,576)	0.050	0.69	—	+11,430	(18,933)	0.55	—
GM	−2310	(10,364)	-0.026	0.82	—	+358	(10,530)	0.97	—
WM	+7876	(9012)	+0.11	0.38	—	+9352	(9207)	0.31	—
sMRI, Analysis B									
Hippocampus, Left	−24.1	(62.9)	−0.04	0.70	—	−18.8	(64.5)	0.77	—
Hippocampus, Right	−15.5	(67.6)	−0.02	0.82	—	−15.0	(69.4)	0.83	—
sMRI, Analysis C									
White matter lesion volume, **Log_e transformed**	+1.29	(1.05)	0.16	0.22	—	+1.59	(1.07)	0.14	—

Key: Age_{v1}, age measured at HANDLS visit 1 (2004–2009); FDR, false discovery rate; GM, gray matter; HANDLS, Healthy Aging in Neighborhoods of Diversity Across the Life Span; HANDLS-SCAN, brain magnetic resonance imaging scan ancillary study of HANDLS; NfL, neurofilament light; SE, standard error; sMRI, structural magnetic resonance imaging; v_1, visit 1 of HANDLS (2004–2009); v_2, visit 2 of HANDLS (2009–2013); v_{scan}, HANDLS-SCAN visit (2011–2015); WM, white matter.

[a] Values are adjusted linear regression coefficients β with associated SE, standardized beta, uncorrected *p* values, corrected q-values (false discovery rate) and results of sensitivity analysis. (N) is the sample size in each analysis. Standardized betas are computed as SD in outcome per SD in Nfl at v2. Q-values presented only for uncorrected *p* values < 0.05 for model 1. Model 1 was adjusted for Age_{v1}, sex, race, poverty status, intracranial volume (*Analyses B* and *C*) and time of follow-up between visit 1 and v_{scan}. Volumes are expressed in mm^3.

[b] Model 2 is a sensitivity analysis further adjusting Model 1 for BMI at visit 1 after screening using machine learning techniques (See Supplemental methods 2).

up, overall (β = +2.131 ± 0.660, b = +0.29, $p = 0.001$, and q = 0.0029). This association was largely unaltered with the addition of other covariates, including v_1 BMI (Table 2, Model 2), or other upstream potentially confounding variables, including measures of kidney and liver diseases (Table S3, Model 3–6). This association was also significantly stronger among females, particularly in models adjusting for visit 1 BMI ($p_{sex \times NfL(v1)} = 0.007$). In fact, in Model 2 among females, $NfL_{(v1)}$ exposure 1 unit increase was linked to a 4-point increase in Log_e transformed WMLV, $p = 0.001$. This association remained largely unaltered in models further adjusted for upstream covariates (Table S3, Models 3–6).

When examining plasma NfL exposure at visit 2, with an average of ∼1.1-year follow-up to sMRI outcome, $NfL_{(v2)}$ was linked to smaller hippocampal volumes in general, with the left hippocampus showing a slightly stronger effect size compared with the right hippocampus, overall (b = −0.19 vs. b = −0.14, respectively, and q < 0.05). More specifically, 1 unit increase in Log_e transformed NfL at v_2 was linked to a left hippocampal volume that was lower by 125 mm^3 in the overall sample ($p = 0.004$ and q = 0.015), an association that was not altered by the addition of other baseline covariates, including v_1 BMI (Table 3, Model 2 and Models 3–6 in Table S4). This association was also mainly detected in males even though heterogeneity of this effect by sex was not detected ($p > 0.05$ for interaction term sex × $NfL_{(v2)}$ in a separate unstratified model).

Our exploratory analyses stratified by race, as shown in Tables S5 and S6, indicated that those main associations of NfL with WMLV and hippocampal volumes were largely homogeneous across racial groups. In contrast, there was significant heterogeneity detected in the relationship between $NfL_{(v1)}$ and TBV, GM, and WM volumes; an inverse association was found among African American but not among White participants in most models, particularly those adjusted for diabetes and serum glucose (Model 3). Sensitivity analyses using the largest available samples for each analysis did not alter our main findings (data not shown). Most notably, a 1 unit increase in NfL exposure at v_1 (Log_e transformed) was associated with a 1.93-unit increase in the Log_e transformed WMLV outcome, overall (β = +1.93 ± 0.60, $p = 0.001$, b = 0.27, and n = 197), an association that was significantly stronger in females (β = +2.37, $p = 1.00$, b = 0.020, and n = 107) and remained significant with adjustment for BMI and other potential confounders. Moreover, a more proximal NfL exposure at v_2 1 unit increase was linked to an average of 115 mm^3 smaller left hippocampal volume outcome (β = −115.2 ± 39.1, $p = 0.004$, b = −0.17, and n = 213, for Model 1). These results were comparable for the right hippocampus, were stronger in men, and slightly altered with the addition of other covariates to Model 1. Both left and right hippocampal volumes were smaller when NfL exposure was "tracking high" over time, by retaining a value greater than 8 pg/mL, overall and among males (Table S7), a relationship not

Table 4
Minimally adjusted and BMI-adjusted associations from *Analyses A* (global GM and WM volumes), *A′* (regional cortical GM/WM), *B* (hippocampal volume), and *C* (white matter lesion volume) versus annualized change in Log_e transformed NfL (empirical Bayes estimator; δNfL_{bayes}) and visit 1 NfL, Log_e transformed or NfL_{v1}: ordinary least square analyses; HANDLS 2004–2013 and HANDLS-SCAN 2011–2015[a]

	Model 1: Minimally adjusted				Model 2: BMI-adjusted, sensitivity analysis (SA)[b]		
	β1	(SE1)	b1	*p*1	β2	(SE2)	*P*2
Total sample (N = 179)							
sMRI, Analysis A							
Total brain							
δNfL_{bayes}	−33,686	(96825)	−0.021	0.73	−46,622	(31,050)	0.14
NfL_{v1}	−3137	(17005)	−0.015	0.85	−2145	(5628)	0.70
GM							
δNfL_{bayes}	−31,771	(51,863)	−0.036	0.54	−38,370	(26,728)	0.15
NfL_{v1}	−7738	(9109)	−0.063	0.40	−6603	(4845)	0.18
WM							
δNfL_{bayes}							
NfL_{v1}	−16,424	(47,153)	−0.023	0.73	−22,022	(22,517)	0.33
sMRI, Analysis B	1186	(8281)	+0.012	0.89	1126	(4082)	0.78
Hippocampus, Left							
δNfL_{bayes}	**−894**	**(310)**	**−0.172**	**0.004**	**−899**	**(310)**	**0.004**
NfL_{v1}	*−104*	*(55)*	*−0.144*	*0.056*	*−95*	*(56)*	*0.094*
Hippocampus, Right							
δNfL_{bayes}	**−725**	**(323)**	**−0.130**	**0.026**	**−731**	**(324)**	**0.024**
NfL_{v1}	−84	(57)	−0.111	0.14	−73	(59)	0.22
Analysis C							
White matter lesion volume, **Log_e transformed**							
δNfL_{bayes}	−2.55	(4.02)	−0.050	0.53	−2.67	(4.02)	0.51
NfL_{v1}	**+1.97**	**(0.71)**	**0.271**	**0.006**	**+2.21**	**(0.73)**	**0.003**

Key: Age_{v1}, age measured at HANDLS visit 1 (2004–2009); δNfL_{bayes}, annualized rate of change in NfL, empirical Bayes estimator; FDR, false discovery rate; GM, gray matter; HANDLS, Healthy Aging in Neighborhoods of Diversity Across the Life Span; HANDLS-SCAN, brain magnetic resonance imaging scan ancillary study of HANDLS; NfL, neurofilament light; SE, standard error; sMRI, structural magnetic resonance imaging; v_1, visit 1 of HANDLS (2004–2009); v_2, visit 2 of HANDLS (2009–2013); v_{scan}, HANDLS-SCAN visit (2011–2015); WM, white matter.

[a] Values are adjusted linear regression coefficients β with associated SE, standardized beta, uncorrected *p* values, and results of sensitivity analysis. (N) is the sample size in each analysis. Standardized betas are computed as SD in outcome per SD in Nfl exposures. Model 1 was adjusted for Age_{v1}, sex, race, poverty status, intracranial volume (*Analyses B* and *C*), and time of follow-up between visit 1 and v_{scan}. Volumes are expressed in mm^3.

[b] Model 2 is a sensitivity analysis further adjusting Model 1 for BMI at visit 1 after screening using machine learning techniques (see Supplemental methods 2).

detected among females. For instance, the left hippocampal volume was ∼138 mm^3 smaller in the chronically elevated NfL group compared to the rest of the sample (β = −138 ± 51 and $p = 0.007$, Model 1), overall. Conversely, tracking low for NfL exposure (i.e. ≤8 pg/mL) trended toward an inverse relationship with WMLV outcome among females in most models, particularly models adjusted for BMI (Model 2: β = −2.20 ± 1.02 and $p = 0.035$) (Table S7).

In another set of secondary models (Table 4), annualized change in NfL (δNfL_{bayes}) was associated with smaller hippocampal volumes in the total population, in both the reduced and the BMI-adjusted models, independently of NfLv1. In contrast, NfLv1 was the main exposure associated with greater WMLV at follow-up, independently of δNfL_{bayes}.

Key findings were largely unaltered in the subsample that was free from head injuries and was deemed as having normal cognition at v_1. Most notably, overall (n = 163), Nfl at v1 exposure was positively associated with WMLV in both the reduced (β ± SE: 2.57 ± 0.76 and $p = 0.001$) and BMI-adjusted models (β ± SE: 2.87 ± 0.79 and $p < 0.001$), with significant interaction by sex and stronger effects among females. However, the association between NfL at v_2 and left hippocampal volumes was attenuated in this selected sample (n = 163), with this exclusion with most results indicating a marginally significant association across models, reflecting a smaller hippocampal volume with higher NfL at v_2 ($p < 0.10$). Findings stratified by race were also comparable between the two samples (N = 163 vs. N = 179) for both NfL at v_1 and v_2. All main and sensitivity analysis output will be made available on the GitHub link: https://github.com/baydounm/HANDLS_NFL_SMRI_PAPER_SUPPDATA.

Finally, when regional small ROI-specific WMLV was left untransformed, results remained similar with respect to main regions affected by elevated NfL levels at baseline. The statistically significant ROI-specific WMLV results (cubic root transformed) at type I error of 0.05 are presented in Table S8 and Fig. 2. Most notably, the top two hits with effect sizes > 0.25 were the right posterior limb of the internal capsule WMLV (b = 0.38 and $p < 0.001$) and right frontal lobe WMLV (b = 0.26 and $p = 0.002$).

4. Discussion

4.1. Summary of findings

This study is among a few to examine the relationships of plasma NfL concentrations at two consecutive visits (v_1 and v_2) with key structural brain MRI markers, including hippocampal, global, and cortical regional brain volumes, and WMLV, in a racially and socioeconomically diverse sample of urban adults. Among key findings, $NfL_{(v1)}$ was significantly associated with larger WMLV at a 5 to 6-year follow-up period. This association was stronger in females. For the short time ∼1-year follow-up, elevated NfL levels were significantly associated with a smaller hippocampal volume. Specifically, and in the overall sample, a 1 unit increase in Log_e transformed NfL at v_2 was linked to a left hippocampal volume that was lower by 125 mm^3, a pattern observed for annualized longitudinal change in NfL (δNfL_{bayes}). Interestingly, this association was mainly detected in males. Most of these associations were not altered by adjusting for biomedical and lifestyle factors. Among African American adults

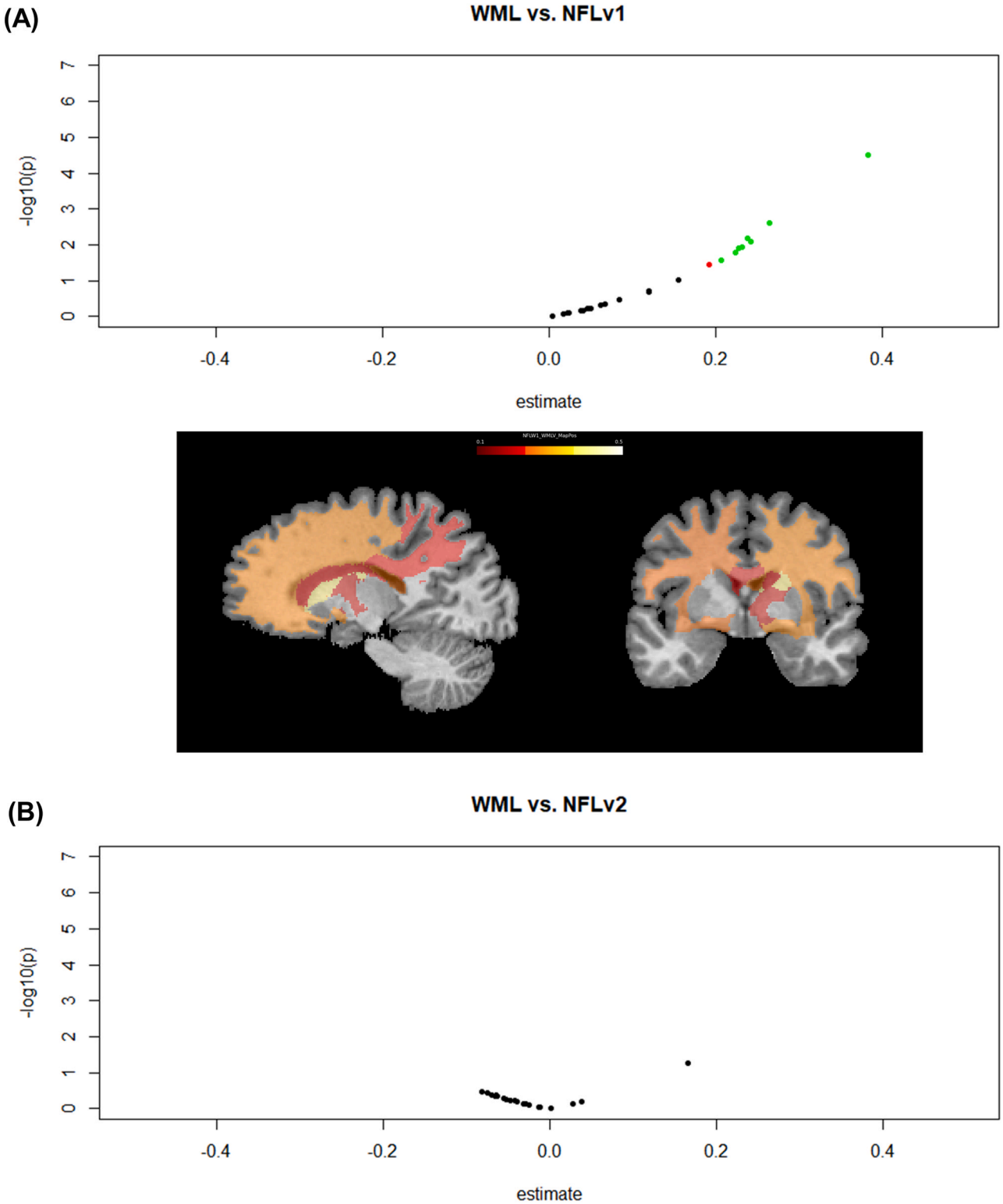

Fig. 2. Volcano plots and brain images of WMLV versus (A) NfL(v_1) and (B) NfL (v_2): HANDLS 2004–2009/2009–2013 and HANDLS-SCAN 2011–2015 (In both the volcano plot and the brain images: values are effect sizes from adjusted linear regression models with $NfL_{(v1)}$ and $NfL_{(v2)}$ (Log_e transformed and z-scored) as alternative exposures and outcomes being regional small ROI WMLV, cubic root transformed. The Log_e transformed value was then z-scored. The multiple linear models were adjusted for age, race, poverty status, time of follow-up between visit 1 and v_{scan}, and the intracranial volume. The volcano plot represents the results of the two models for each exposure, with outcomes being regional small ROI WMLVs. "Estimate" refers to the standardized beta coefficient or effect size; −Log10(p) is the associated negative Log base 10 of the p value for each regional association. Red dots represent p 0.05 with b +0.20 for positive associations or b > −0.20 for negative associations; green dots represent p 0.05 with b > +0.20 for positive associations or b −0.20 for negative associations. The brain images represent the same results using FSLEYES software for visualizing effect sizes. Those effect sizes were selected for regions with p 0.05, using a color gradient. Colder (blue) colors are for negative associations (smaller WMLV with higher NfL exposure), and warmer colors (red through yellow) are for positive associations (larger WMLV with higher NfL exposure). Lighter colors indicate stronger effect sizes.) Abbreviations: HANDLS, Healthy Aging in Neighborhoods of Diversity Across the Life Span; HANDLS-SCAN, HANDLS brain MRI ancillary study; MRI, magnetic resonance imaging; WMLV, white matter lesion volume.

only, NfL_{v1} was inversely related to total, gray and white matter volumes.

4.2. Previous human studies

Currently, methods for diagnosing and monitoring neuropathology rely on expensive imaging modalities that have limited availability. CSF biomarkers, which include NfL, have also been used but require invasive procedures. Accordingly, less invasive biomarkers of neuroaxonal damage and neurocognitive decline are needed to identify individuals at risk for AD and other neurodegenerative diseases. Data indicate that plasma NfL may be a suitable option for a biomarker. Recent technological advances indicate that NfL levels measured in blood, i.e., plasma NfL, are associated with AD diagnosis and various cognitive, imaging, and biochemical disease measures (Jin et al., 2019; Mattsson et al., 2017; Zhao et al., 2019). CSF NfL inversely associates with clinical dementia rating scale scores, the recognition memory test (Weston et al., 2019), and the cognitive subscale of an AD assessment battery (Mattsson et al., 2019) is elevated in the early stages of dementia and is a strong predictor for cognitive decline in Aβ positive individuals (Bos et al., 2019) and in the general nondemented older adult population (Merluzzi et al., 2019). Given that Aβ positivity alone was not sufficient for predicting symptoms of cognitive decline in AD, identifying additional markers of neurodegeneration downstream from Aβ accumulation is highly useful for screening individuals in presymptomatic trials (Weston et al., 2019).

Recent reports suggest differences in levels of plasma NfL even in early stages of AD. For example, plasma NfL levels are elevated based on underlying pathology (Aβ+ vs. Aβ-) in adults with subjective cognitive decline (SCI), MCI, and AD (Giacomucci et al., 2022). Furthermore, in a cross-sectional study, elevated plasma NfL levels were reported in SCI-Aβ+ patients compared to normal controls with Aβ- and correlated with brain amyloid and cognitive decline (Huang et al., 2022). Plasma NfL was predictive of longitudinal cognitive decline in SCI and MCI patients (Bangen et al., 2021) and in acute poststroke patients with subjective cognitive decline (Wang et al., 2021). Therefore, plasma NfL levels may be a useful marker not only of the stage of cognitive decline but also of the underlying pathology, thus being suitable as a biomarker in the early stages of AD.

Because of the strong association between plasma and CSF NfL levels, and the invasiveness of acquiring CSF, plasma NfL may be a better screening tool. This is supported by evidence that plasma NfL may accurately predict the estimated year of onset for dementia in familial and autosomal dominant AD (Sanchez-Valle et al., 2018; Weston et al., 2017). Also, recent studies have shown that serum or plasma NfL are direct indicators of axonal degeneration based on neuroimaging markers, including gray and white matter pathologies (Jakimovski et al., 2019; Mielke et al., 2019; Sun et al., 2020), acting as proxies for hypometabolism in AD-vulnerable brain regions, particularly in Aβ-positive individuals (Benedet et al., 2019). Generally, axonal demyelination triggers inefficient energy utilization, mitochondrial dysfunction, and oxidative stress accumulation, alterations that increase axonal fragmentation resulting in neurodegeneration (Fischer et al., 2013). Such pathology can spread at independent tract locations and their associated gray matter structures (Bergsland et al., 2017). Since such axonal retraction does not often occur instantaneously, it is more likely that baseline plasma NfL rather than follow-up or change in NfL is associated with change or follow-up outcomes of neurodegeneration or adverse cognitive performance (Jakimovski et al., 2019; Trapp et al., 1998). This is in line with our current findings.

As plasma NfL is a marker of neuroaxonal damage, recent data suggest that, in addition to having potential clinical utility in neurodegenerative diseases, blood NfL may also be a useful indicator of neuronal injury due to cerebrovascular disease. Here, we found that elevated NfL_{v1} was associated with greater WMLV. WM lesions reflect small vessel disease, which is a highly prevalent brain pathology causing vascular cognitive impairment, stroke, and mortality (Pantoni, 2010). Moreover, serum NfL was higher in patients with genetically defined and sporadic small vessel disease and associated with greater MRI mean diffusivity, WM hyperintensity volume, lacune volume, and microbleed count(Duering et al., 2018). Patients with vascular dementia had higher levels of serum NfL compared to controls (Yuan et al., 2020), and after ischemic stroke, serum NfL levels were associated with secondary degeneration of white matter tracts (Tiedt et al., 2018) and WMLV (Uphaus et al., 2019). Therefore, plasma NfL may be linked to future subclinical brain pathologies that increase the risk for disability and mortality. This is important, given that imaging modalities are costly and require specialized machinery and personnel, and detailed postimaging analysis. Our cohort notably consists of middle-aged African American and White adults without a history of cerebrovascular or neurodegenerative diseases, suggesting that plasma NfL shows promise as a biomarker for future brain pathologies in the absence of previous diagnoses. In previous secondary analyses of a comparable sample of HANDLS SCAN participants, we show that adverse volumetric outcomes considered in this study are associated with a decline in cognitive performance over time in several domains of cognition, including v_1 and v_2 cognitive measurements, which preceded the HANDLS SCAN visit (see supplemental methods 4 in Beydoun et al., 2021a). More specifically, that study indicated that a slower decline over time for certain cognitive domains was associated with larger MRI scan volumes in the region of the hippocampus, along with smaller WMLV and larger cortical brain volumes (Beydoun et al., 2021a). In particular, larger hippocampal volumes were associated with slower decline based on the test of visual memory and attention, whereas faster decline based on an executive function test was related to larger WMLV, especially among African American adults (Beydoun et al., 2021a). WM volume at follow-up, particularly among men, was related to a slower decline on the Digit Span Forward test, reflecting the attention domain of cognitive function (Beydoun et al., 2021a). Conversely, faster decline in executive function was linked to smaller temporal GM cortical volumes (Beydoun et al., 2021a).

In our short-term follow-up analyses of NfL_{v2} with MRI-based assessed subclinical brain pathology, we found that NfL was strongly associated with smaller hippocampal volumes. As hippocampal atrophy is associated with cognitive decline and dementia, particularly AD (Hsu et al., 2018; Walter et al., 2019), these findings lay important groundwork for identifying factors that may be linked to subclinical brain volume changes. In agreement with this idea, in analyses of an aging cohort from the Austrian Stroke Prevention Family Study, serum NfL was associated with smaller brain volume and future brain atrophy (Khalil et al., 2020). In a cohort of Hispanic and non-Hispanic adults with cognitive impairment, the etiology of which is due to many diverse neurodegenerative diseases, serum NfL was associated with hippocampal atrophy (Barker et al., 2021). In longitudinal analyses, higher baseline plasma NfL was associated with a longitudinal decline in hippocampal volume (Mielke et al., 2019; Rajan et al., 2020). Altogether, these studies suggest associations between blood NfL levels and changes in brain volume, which could, in turn, influence neuropsychological functioning. It is possible that the main reason that we did not detect an association between medium-term NfL and hippocampal volume is that there is

a threshold effect beyond which NfL can affect this volume and earlier NfL tended to be lower than later NfL in this cohort.

4.3. Strengths and limitations

This study has several strengths, including its novel examination of relationships between markers of neuroaxonal damage and brain structural sMRI measures, which reflect global and regional volumes and WMLV, potentially underlying various neuropathologies. Despite being cross-sectional in design, this study provided 5–6 years of latency between NfL exposure and outcome (brain MRI measures) while considering shorter term NfL measured 1–2 years prior to follow-up as an additional exposure of interest, in addition to "tracking high," "tracking low," and annualized change in NfL as secondary longitudinal exposures. Furthermore, given the importance of sex in both NfL and cognitive impairment, we examined these hypotheses separately among males and females, and adjusted basic models for multiple testing and potential confounders for sociodemographic, lifestyle, and health-related factors, including hematological and other nutritional biomarkers. These analyses also considered heterogeneity of associations by race, which is important given the disparities in risk of vascular dementia, cognitive decline, and AD between African American and White adults (Matthews et al., 2019). Importantly, our cohort is relatively young and free from neurological and cerebrovascular diseases, indicating that plasma NfL can be equally useful for monitoring brain health in middle-aged adults. Our study findings did indicate that there was some heterogeneity across sex and race, in the association between plasma NfL and adverse brain volumetric outcomes, though this heterogeneity was outcome-specific.

Nevertheless, our study has several limitations. First, latency between exposure and outcome may render findings speculative as opposed to a cohort study with repeated outcomes, allowing testing of baseline exposure against annualized change in outcome. This latency period between exposure and outcome differed among participants though it had a central tendency of 5–6 years.

Thus, we controlled for the follow-up time in our models. Moreover, the lack of baseline sMRI measure should be addressed in future studies of similar populations, and future longitudinal studies should examine change in volumetric outcomes in relation to short- and medium-term NfLs or in relation to tracking high versus low NfL and estimated annualized change in NfL. Second, although we did not directly assess cognitive decline along with volumetric outcomes, a previous study of ours conducted this secondary analysis, confirming that the selected volumetric outcomes are reflective of cognitive decline over time and its results were summarized earlier (Beydoun et al., 2021a). Third, residual confounding is a potential problem given the observational nature of this study. Fourth, our study did not have a large enough sample on APOE genotype or other plasma neurodegeneration markers to conduct analyses with those markers included as either potential confounders or effect modifiers. Finally, our findings are in middle-aged urban White and African American adults, which may limit the generalizability to older elderly populations.

5. Conclusions

In summary, baseline plasma NfL was consistently associated with larger WMLV, particularly among females. On the other hand, follow-up and annualized longitudinal changes in plasma NfL were both linked to smaller bilateral hippocampal volumes, overall, with a stronger effect found in the left hippocampal volume and among males. Among African American adults, $NfL_{(v1)}$ was inversely related to total, gray and white matter volumes. These associations were robust to further adjustment with key potential confounders. Thus, plasma NfL may be an independent marker for a medium-term increase in lesion volumes, while its increase over time and its elevation in the shorter term may potentially be a marker for smaller hippocampal volumes normalized to the ICV independently of other confounding factors. It may also reflect future smaller cortical volumes among African American adults. Therefore, plasma NfL may be a promising biomarker to reflect future subclinical brain pathologies in middle-aged adults.

Ethical approval and consent to participate

All participants provided written informed consent at each wave of the Healthy Aging in Neighborhoods of Diversity across the Life Span (HANDLS) study. The study protocol was reviewed and approved by the National Institutes of Health Institutional Review Board, protocol number 09-AG- N248.

Sources of funding

This work was supported in part by the Intramural Research Program of the NIH, National Institute on Aging. This work was also supported by the National Institutes of Health, R01-AG034161 and P30 AG028747–14S1 to S.R.W, ZIA–AG000513 to M.K.E. and A.B.Z., and The University of Maryland Claude D. Pepper Older Americans Independence Center (NIH grant P30 AG028747).

Submission date: April 5th, 2023.

Consent for publication

Not applicable.

Competing interests and disclaimers

All authors declare no conflict of interest. The views expressed in this article are those of the authors and do not necessarily reflect the official policy or position of the Fort Belvoir Community Hospital, the Defense Health Agency, the Department of Defense, or the U.S. Government. Reference to any commercial products within this publication does not create or imply any endorsement by the Fort Belvoir Community Hospital, the Defense Health Agency, the Department of Defense, or the U.S. Government.

CRediT authorship contribution statement

All authors reviewed the manuscript. MAB: conceptualization, plan of analysis, statistical analysis, literature review, write-up of parts of the manuscript, and revision of the manuscript. NNH: conceptualization, data acquisition, plan of analysis, literature search and review, write-up of parts of the manuscript, and revision of the manuscript. HAB: plan of analysis, assistance with statistical analysis, literature search and review, write-up of parts of the manuscript, and revision of the manuscript. JW: plan of analysis, assistance with statistical analysis, literature search and review, assistance with statistical analysis, write-up of parts of the manuscript, and revision of the manuscript. AIM: plan of analysis, literature search and review, write-up of parts of the manuscript, and revision of the manuscript. LIK: data acquisition, literature search and review, write-up of parts of the manuscript, and revision of the manuscript. CD: data acquisition, plan of analysis, write-up of parts of the manuscript, and revision of the manuscript. RPG: data acquisition, plan of analysis, write-up of parts of the manuscript, and revision of the manuscript. SLS: data acquisition, plan of analysis, write-up of parts of the manuscript, and revision of the manuscript. GE: data acquisition, plan of analysis, assistance with data management and statistical analysis, prepared parts of Fig. 2, write-up of parts of the

manuscript, and revision of the manuscript. MKE: data acquisition, plan of analysis, write-up of parts of the manuscript, and revision of the manuscript. ABZ: data acquisition, data management, plan of analysis, write-up of parts of the manuscript, and revision of the manuscript. SRW: conceptualization, data acquisition, data management, plan of analysis, write-up of parts of the manuscript, and revision of the manuscript.

Availability of data and materials

The study protocol (09-AG-N248) received approval from the National Institute on Environmental Health Sciences' Institutional Review Board (IRB) of the National Institutes of Health (NIH). Upon request, data can be made available to researchers with approved proposals, after they have agreed to confidentiality as required by our IRB. Policies are publicized on https://handls.nih.gov. Data access request can be sent to principal investigators (PIs) or the study manager, Jennifer Norbeck at norbeckje@mail.nih.gov.

Acknowledgements

This study was supported by the Intramural Research Program of the National Institute on Aging, National Institutes of Health. The authors would like to thank all HANDLS and HANDLS SCAN participants, staff, and investigators for their contributions to this study. The authors would like to thank Ms. Nicolle Mode for her contribution in selecting participants for plasma NfL analyses and related data management.

Verification

The author declare no conflict of interest for (a), (b), or (c). This research was supported entirely by the Intramural Research Program of the NIH and National Institute on Aging. This manuscript was not submitted or published elsewhere. This manuscript was exempted from a full protocol by the National Institute on Aging's IRB and has received approval. All authors have indeed reviewed the contents of the manuscript being submitted, approved its contents, and validated the accuracy of the data.

Appendix A. Supporting information

Supplementary data associated with this article can be found in the online version at doi:10.1016/j.neurobiolaging.2023.04.013.

References

Bangen, K.J., Thomas, K.R., Weigand, A.J., Edmonds, E.C., Clark, A.L., Solders, S., Delano-Wood, L., Galasko, D.R., Bondi, M.W., Alzheimer's Disease Neuroimaging, I., 2021. Elevated plasma neurofilament light predicts a faster rate of cognitive decline over 5 years in participants with objectively-defined subtle cognitive decline and MCI. Alzheimers Dement. 17 (10), 1756–1762.

Barker, W., Quinonez, C., Greig, M.T., Behar, R., Chirinos, C., Rodriguez, R.A., Rosselli, M., Rodriguez, M.J., Cid, R.C., Rundek, T., McFarland, K., Hanson, K., Smith, G., DeKosky, S., Vaillancourt, D., Adjouadi, M., Marsiske, M., Ertekin-Taner, N., Golde, T., Loewenstein, D.A., Duara, R., 2021. Utility of plasma neurofilament light in the 1Florida Alzheimer's Disease Research Center (ADRC). J. Alzheimers Dis. 79 (1), 59–70.

Benedet, A.L., Ashton, N.J., Pascoal, T.A., Leuzy, A., Mathotaarachchi, S., Kang, M.S., Therriault, J., Savard, M., Chamoun, M., Scholl, M., Zimmer, E.R., Gauthier, S., Labbe, A., Zetterberg, H., Blennow, K., Neto, P.R., 2019. Plasma neurofilament light associates with Alzheimer's disease metabolic decline in amyloid-positive individuals. Alzheimers Dement. (Amst.) 11, 679–689.

Bergsland, N., Tavazzi, E., Lagana, M.M., Baglio, F., Cecconi, P., Viotti, S., Zivadinov, R., Baselli, G., Rovaris, M., 2017. White matter tract injury is associated with deep gray matter iron deposition in multiple sclerosis. J. Neuroimaging 27 (1), 107–113.

Beydoun, M.A., Hossain, S., MacIver, P.H., Srinivasan, D., Beydoun, H.A., Maldonado, A.I., Katzel, L.I., Davatzikos, C., Gullapalli, R.P., Seliger, S.L., Erus, G., Evans, M.K., Zonderman, A.B., Waldstein, S.R., 2021a. Red cell distribution width, anemia, and brain volumetric outcomes among middle-aged adults. J. Alzheimers Dis. 81 (2), 711–727.

Beydoun, M.A., Noren Hooten, N., Beydoun, H.A., Maldonado, A.I., Weiss, J., Evans, M.K., Zonderman, A.B., 2021b. Plasma neurofilament light as a potential biomarker for cognitive decline in a longitudinal study of middle-aged urban adults. Transl. Psychiatry 11 (1), 436.

Bos, I., Vos, S., Verhey, F., Scheltens, P., Teunissen, C., Engelborghs, S., Sleegers, K., Frisoni, G., Blin, O., Richardson, J.C., Bordet, R., Tsolaki, M., Popp, J., Peyratout, G., Martinez-Lage, P., Tainta, M., Lleo, A., Johannsen, P., Freund-Levi, Y., Frolich, L., Vandenberghe, R., Westwood, S., Dobricic, V., Barkhof, F., Legido-Quigley, C., Bertram, L., Lovestone, S., Streffer, J., Andreasson, U., Blennow, K., Zetterberg, H., Visser, P.J., 2019. Cerebrospinal fluid biomarkers of neurodegeneration, synaptic integrity, and astroglial activation across the clinical Alzheimer's disease spectrum. Alzheimers Dement. 15 (5), 644–654.

de Wolf, F., Ghanbari, M., Licher, S., McRae-McKee, K., Gras, L., Weverling, G.J., Wermeling, P., Sedaghat, S., Ikram, M.K., Waziry, R., Koudstaal, W., Klap, J., Kostense, S., Hofman, A., Anderson, R., Goudsmit, J., Ikram, M.A., 2020. Plasma tau, neurofilament light chain and amyloid-beta levels and risk of dementia; a population-based cohort study. Brain 143 (4), 1220–1232.

Doshi, J., Erus, G., Ou, Y., Resnick, S.M., Gur, R.C., Gur, R.E., Satterthwaite, T.D., Furth, S., Davatzikos, C., Alzheimer's Neuroimaging, I., 2016. MUSE: MUlti-atlas region Segmentation utilizing Ensembles of registration algorithms and parameters, and locally optimal atlas selection. Neuroimage 127, 186–195.

Doshi, J., Erus, G., Ou, Y., Davatzikos, C. Ensemble-based medical image labeling via sampling morphological appearance manifolds. MICCAI Challenge Workshop on Segmentation: Algorithms, Theory and Applications, 2013.

Duering, M., Konieczny, M.J., Tiedt, S., Baykara, E., Tuladhar, A.M., Leijsen, E.V., Lyrer, P., Engelter, S.T., Gesierich, B., Achmuller, M., Barro, C., Adam, R., Ewers, M., Dichgans, M., Kuhle, J., de Leeuw, F.E., Peters, N., 2018. Serum neurofilament light chain levels are related to small vessel disease burden. J. Stroke 20 (2), 228–238.

Egle, M., Loubiere, L., Maceski, A., Kuhle, J., Peters, N., Markus, H.S., 2021. Neurofilament light chain predicts future dementia risk in cerebral small vessel disease. J. Neurol. Neurosurg. Psychiatry 92 (6), 582–589.

Evans, M.K., Lepkowski, J.M., Powe, N.R., LaVeist, T., Kuczmarski, M.F., Zonderman, A.B., 2010. Healthy aging in neighborhoods of diversity across the life span (HANDLS): overcoming barriers to implementing a longitudinal, epidemiologic, urban study of health, race, and socioeconomic status. Ethn. Dis. 20 (3), 267–275.

Fischer, M.T., Wimmer, I., Hoftberger, R., Gerlach, S., Haider, L., Zrzavy, T., Hametner, S., Mahad, D., Binder, C.J., Krumbholz, M., Bauer, J., Bradl, M., Lassmann, H., 2013. Disease-specific molecular events in cortical multiple sclerosis lesions. Brain 136 (Pt 6), 1799–1815.

Folstein, M.F., Folstein, S.E., McHugh, P.R., 1975. "Mini-mental state". A practical method for grading the cognitive state of patients for the clinician. J. Psychiatr. Res. 12 (3), 189–198.

Giacomucci, G., Mazzeo, S., Bagnoli, S., Ingannato, A., Leccese, D., Berti, V., Padiglioni, S., Galdo, G., Ferrari, C., Sorbi, S., Bessi, V., Nacmias, B., 2022. Plasma neurofilament light chain as a biomarker of Alzheimer's disease in Subjective Cognitive Decline and Mild Cognitive Impairment. J. Neurol. 269 (8), 4270–4280.

He, L., Barreto, de Souto, Aggarwal, P., Nguyen, G., Morley, A.D., Li, J.E., Bateman, Y., Vellas, R.J., Group, M.D, B., 2020. Plasma Abeta and neurofilament light chain are associated with cognitive and physical function decline in non-dementia older adults. Alzheimers Res. Ther. 12 (1), 128.

Hsu, F.C., Sink, K.M., Hugenschmidt, C.E., Williamson, J.D., Hughes, T.M., Palmer, N.D., Xu, J., Smith, S.C., Wagner, B.C., Whitlow, C.T., Bowden, D.W., Maldjian, J.A., Divers, J., Freedman, B.I., 2018. Cerebral structure and cognitive performance in African Americans and European Americans with type 2 diabetes. J. Gerontol. A Biol. Sci. Med. Sci. 73 (3), 407–414.

Huang, Y., Li, Y., Xie, F., Guo, Q., 2022. Associations of plasma phosphorylated tau181 and neurofilament light chain with brain amyloid burden and cognition in objectively defined subtle cognitive decline patients. CNS Neurosci. Ther. 28 (12), 2195–2205.

Jakimovski, D., Kuhle, J., Ramanathan, M., Barro, C., Tomic, D., Hagemeier, J., Kropshofer, H., Bergsland, N., Leppert, D., Dwyer, M.G., Michalak, Z., Benedict, R.H.B., Weinstock-Guttman, B., Zivadinov, R., 2019. Serum neurofilament light chain levels associations with gray matter pathology: a 5-year longitudinal study. Ann. Clin. Transl. Neurol. 6 (9), 1757–1770.

Jenkinson, M., Bannister, P., Brady, M., Smith, S., 2002. Improved optimization for the robust and accurate linear registration and motion correction of brain images. Neuroimage 17 (2), 825–841.

Jenkinson, M., Smith, S., 2001. A global optimisation method for robust affine registration of brain images. Med. Image Anal. 5 (2), 143–156.

Jin, M., Cao, L., Dai, Y.P., 2019. Role of neurofilament light chain as a potential biomarker for Alzheimer's disease: a correlative meta-analysis. Front. Aging Neurosci. 11, 254.

Jonsson, M., Zetterberg, H., van Straaten, E., Lind, K., Syversen, S., Edman, A., Blennow, K., Rosengren, L., Pantoni, L., Inzitari, D., Wallin, A., 2010. Cerebrospinal fluid biomarkers of white matter lesions - cross-sectional results from the LADIS study. Eur. J. Neurol. 17 (3), 377–382.

Khalil, M., Pirpamer, L., Hofer, E., Voortman, M.M., Barro, C., Leppert, D., Benkert, P., Ropele, S., Enzinger, C., Fazekas, F., Schmidt, R., Kuhle, J., 2020. Serum neurofilament light levels in normal aging and their association with morphologic brain changes. Nat. Commun. 11 (1), 812.

Khalil, M., Teunissen, C.E., Otto, M., Piehl, F., Sormani, M.P., Gattringer, T., Barro, C., Kappos, L., Comabella, M., Fazekas, F., Petzold, A., Blennow, K., Zetterberg, H., Kuhle, J., 2018. Neurofilaments as biomarkers in neurological disorders. Nat. Rev. Neurol. 14 (10), 577–589.

Kuhle, J., Barro, C., Andreasson, U., Derfuss, T., Lindberg, R., Sandelius, A., Liman, V., Norgren, N., Blennow, K., Zetterberg, H., 2016. Comparison of three analytical platforms for quantification of the neurofilament light chain in blood samples: ELISA, electrochemiluminescence immunoassay and Simoa. Clin. Chem. Lab. Med. 54 (10), 1655–1661.

Lao, Z., Shen, D., Liu, D., Jawad, A.F., Melhem, E.R., Launer, L.J., Bryan, R.N., Davatzikos, C., 2008. Computer-assisted segmentation of white matter lesions in 3D MR images using support vector machine. Acad. Radiol. 15 (3), 300–313.

Matthews, K.A., Xu, W., Gaglioti, A.H., Holt, J.B., Croft, J.B., Mack, D., McGuire, L.C., 2019. Racial and ethnic estimates of Alzheimer's disease and related dementias in the United States (2015–2060) in adults aged ≥65 years. Alzheimers Dement. 15 (1), 17–24.

Mattsson, N., Andreasson, U., Zetterberg, H., Blennow, K., Alzheimer's Disease Neuroimaging, I., 2017. Association of plasma neurofilament light with neurodegeneration in patients with Alzheimer disease. JAMA Neurol. 74 (5), 557–566.

Mattsson, N., Cullen, N.C., Andreasson, U., Zetterberg, H., Blennow, K., 2019. Association between longitudinal plasma neurofilament light and neurodegeneration in patients with Alzheimer disease. JAMA Neurol. 76 (7), 791–799.

Merluzzi, A.P., Vogt, N.M., Norton, D., Jonaitis, E., Clark, L.R., Carlsson, C.M., Johnson, S.C., Asthana, S., Blennow, K., Zetterberg, H., Bendlin, B.B., 2019. Differential effects of neurodegeneration biomarkers on subclinical cognitive decline. Alzheimers Dement. (N. Y.) 5, 129–138.

Mielke, M.M., Syrjanen, J.A., Blennow, K., Zetterberg, H., Vemuri, P., Skoog, I., Machulda, M.M., Kremers, W.K., Knopman, D.S., Jack Jr., C., Petersen, R.C., Kern, S., 2019. Plasma and CSF neurofilament light: relation to longitudinal neuroimaging and cognitive measures. Neurology 93 (3), e252–e260.

Nilsson, I.A.K., Millischer, V., Karrenbauer, V.D., Jureus, A., Salehi, A.M., Norring, C., von Hausswolff-Juhlin, Y., Schalling, M., Blennow, K., Bulik, C.M., Zetterberg, H., Landen, M., 2019. Plasma neurofilament light chain concentration is increased in anorexia nervosa. Transl. Psychiatry 9 (1), 180.

Norgren, N., Rosengren, L., Stigbrand, T., 2003. Elevated neurofilament levels in neurological diseases. Brain Res. 987 (1), 25–31.

Nyberg, L., Lundquist, A., Nordin Adolfsson, A., Andersson, M., Zetterberg, H., Blennow, K., Adolfsson, R., 2020. Elevated plasma neurofilament light in aging reflects brain white-matter alterations but does not predict cognitive decline or Alzheimer's disease. Alzheimers Dement. (Amst.) 12 (1), e12050.

Pantoni, L., 2010. Cerebral small vessel disease: from pathogenesis and clinical characteristics to therapeutic challenges. Lancet Neurol 9 (7), 689–701.

Peters, N., van Leijsen, E., Tuladhar, A.M., Barro, C., Konieczny, M.J., Ewers, M., Lyrer, P., Engelter, S.T., Kuhle, J., Duering, M., de Leeuw, F.E., 2020. Serum neurofilament light chain is associated with incident lacunes in progressive cerebral small vessel disease. J. Stroke 22 (3), 369–376.

R Foundation for Statistical Computing. 2013. R: a language and environment for statistical computing. Available at: ⟨http://www.R-project.org/⟩ Access date: January 20th, 2023.

Rajan, K.B., Aggarwal, N.T., McAninch, E.A., Weuve, J., Barnes, L.L., Wilson, R.S., DeCarli, C., Evans, D.A., 2020. Remote blood biomarkers of longitudinal cognitive outcomes in a population study. Ann. Neurol. 88 (6), 1065–1076.

Raket, L.L., Kuhnel, L., Schmidt, E., Blennow, K., Zetterberg, H., Mattsson-Carlgren, N., 2020. Utility of plasma neurofilament light and total tau for clinical trials in Alzheimer's disease. Alzheimers Dement. (Amst.) 12 (1), e12099.

Rubsamen, N., Maceski, A., Leppert, D., Benkert, P., Kuhle, J., Wiendl, H., Peters, A., Karch, A., Berger, K., 2021. Serum neurofilament light and tau as prognostic markers for all-cause mortality in the elderly general population-an analysis from the MEMO study. BMC Med. 19 (1), 38.

Sanchez-Valle, R., Heslegrave, A., Foiani, M.S., Bosch, B., Antonell, A., Balasa, M., Llado, A., Zetterberg, H., Fox, N.C., 2018. Serum neurofilament light levels correlate with severity measures and neurodegeneration markers in autosomal dominant Alzheimer's disease. Alzheimers Res. Ther. 10 (1), 113.

Scherling, C.S., Hall, T., Berisha, F., Klepac, K., Karydas, A., Coppola, G., Kramer, J.H., Rabinovici, G., Ahlijanian, M., Miller, B.L., Seeley, W., Grinberg, L.T., Rosen, H., Meredith Jr., J., Boxer, A.L., 2014. Cerebrospinal fluid neurofilament concentration reflects disease severity in frontotemporal degeneration. Ann. Neurol. 75 (1), 116–126.

Shahim, P., Gren, M., Liman, V., Andreasson, U., Norgren, N., Tegner, Y., Mattsson, N., Andreasen, N., Ost, M., Zetterberg, H., Nellgard, B., Blennow, K., 2016. Serum neurofilament light protein predicts clinical outcome in traumatic brain injury. Sci. Rep. 6, 36791.

STATA. 2019. Statistics/data analysis: release 16.0. Stata Corporation, Texas.

Sun, Y., Tan, L, Xu, W., Wang, Z.T., Hu, H., Li, J.Q., Dong, Q., Tan, L., Yu, J.T., Alzheimer's Disease Neuroimaging, I., 2020. Plasma neurofilament light and longitudinal progression of white matter hyperintensity in elderly persons without dementia. J. Alzheimers Dis. 75 (3), 729–737.

Teunissen, C.E., Dijkstra, C., Polman, C., 2005. Biological markers in CSF and blood for axonal degeneration in multiple sclerosis. Lancet Neurol. 4 (1), 32–41.

Tiedt, S., Duering, M., Barro, C., Kaya, A.G., Boeck, J., Bode, F.J., Klein, M., Dorn, F., Gesierich, B., Kellert, L., Ertl-Wagner, B., Goertler, M.W., Petzold, G.C., Kuhle, J., Wollenweber, F.A., Peters, N., Dichgans, M., 2018. Serum neurofilament light: A biomarker of neuroaxonal injury after ischemic stroke. Neurology 91 (14), e1338–e1347.

Trapp, B.D., Peterson, J., Ransohoff, R.M., Rudick, R., Mork, S., Bo, L., 1998. Axonal transection in the lesions of multiple sclerosis. N. Engl. J. Med. 338 (5), 278–285.

Uphaus, T., Bittner, S., Groschel, S., Steffen, F., Muthuraman, M., Wasser, K., Weber-Kruger, M., Zipp, F., Wachter, R., Groschel, K., 2019. NfL (neurofilament light chain) levels as a predictive marker for long-term outcome after ischemic stroke. Stroke 50 (11), 3077–3084.

Waldstein, S.R., Dore, G.A., Davatzikos, C., Katzel, L.I., Gullapalli, R., Seliger, S.L., Kouo, T., Rosenberger, W.F., Erus, G., Evans, M.K., Zonderman, A.B., 2017. Differential associations of socioeconomic status with global brain volumes and white matter lesions in African American and White adults: the HANDLS SCAN study. Psychosom. Med. 79 (3), 327–335.

Walter, S., Dufouil, C., Gross, A.L., Jones, R.N., Mungas, D., Filshtein, T.J., Manly, J.J., Arpawong, T.E., Glymour, M.M., 2019. Neuropsychological test performance and MRI markers of dementia risk: reducing education bias. Alzheimer Dis. Assoc. Disord. 33 (3), 179–185.

Wang, J.H., Huang, J., Guo, F.Q., Wang, F., Yang, S., Yu, N.W., Zheng, B., Wang, J., 2021. Circulating neurofilament light predicts cognitive decline in patients with post-stroke subjective cognitive impairment. Front. Aging Neurosci. 13, 665981.

Weston, P.S.J., Poole, T., O'Connor, A., Heslegrave, A., Ryan, N.S., Liang, Y., Druyeh, R., Mead, S., Blennow, K., Schott, J.M., Frost, C., Zetterberg, H., Fox, N.C., 2019. Longitudinal measurement of serum neurofilament light in presymptomatic familial Alzheimer's disease. Alzheimers Res. Ther. 11 (1), 19.

Weston, P.S.J., Poole, T., Ryan, N.S., Nair, A., Liang, Y., Macpherson, K., Druyeh, R., Malone, I.B., Ahsan, R.L., Pemberton, H., Klimova, J., Mead, S., Blennow, K., Rossor, M.N., Schott, J.M., Zetterberg, H., Fox, N.C., 2017. Serum neurofilament light in familial Alzheimer disease: a marker of early neurodegeneration. Neurology 89 (21), 2167–2175.

Yuan, C., Fondell, E., Ascherio, A., Okereke, O.I., Grodstein, F., Hofman, A., Willett, W.C., 2020. Long-term intake of dietary carotenoids is positively associated with late-life subjective cognitive function in a prospective study in US women. J. Nutr. 150 (7), 1871–1879.

Zhao, Y., Xin, Y., Meng, S., He, Z., Hu, W., 2019. Neurofilament light chain protein in neurodegenerative dementia: a systematic review and network meta-analysis. Neurosci. Biobehav. Rev. 102, 123–138.

Plasma Neurofilament light and brain volumetric outcomes among middle-aged urban adults

Beydoun et. al.

ONLINE SUPPLEMENTARY MATERIAL

Online Supplemental Method 1. Brain structural/volumetric (s) magnetic resonance imaging (MRI) detailed description:

HANDLS description

sMRI

In addition to standard axial T1, T2, FLAIR images, high-resolution axial T1-weighted MPRAGE (TE = 2.32 ms, TR = 1900ms, TI = 900ms, flip angle = 9º, resolution = 256 × 256 × 96, FOV = 230 mm, sl. Thick. = 0.9 mm) of the brain was obtained for structural imaging. We used images as anatomic references and for the extraction of parameters of regional and whole brain volumes. T1-weighted MP-RAGE images covered the whole brain at a thickness of 1.2 mm for 160 sagittal slices (TR/TE/TI=2300/2.9/900 ms; FOV 25.6cm). These images were then converted to axial sections for comparative purposes.

The Section for Biomedical Image Analysis at the University of Pennsylvania developed techniques in-house to preprocess structural MRI scans. First, extra-cranial material on the T1-weighted images was removed using a multi-atlas registration method(Doshi et al., 2013). Bias was corrected using multiplicative intrinsic component optimization (MICO) method (Li et al., 2014). MUlti-atlas region Segmentation utilizing Ensembles (MUSE), segmented the pre-processed images into a set of anatomical regions of interest (ROIs) (Doshi et al., 2016). MUSE integrates a broad ensemble of labeled templates by using a number of warping algorithms, regularization atlases and parameters (Doshi et al., 2016).

Quality assurance

The Core for Translational Research in Imaging @ Maryland (C-TRIM), managed by the Department of Diagnostic Radiology at UMB's School of Medicine, has instituted several quality control measures to ensure highest level of quality and safety. The research-dedicated scanner undergoes routine quality data assurance as mandated by the American College of Radiology(Mulkern et al., 2008). In addition, the AD Neuroimaging Initiative phantom is used to assess weekly signal-to-noise ratio and monthly structural distortions(Gunter et al., 2009). We periodically check the reliability of diffusion data by utilizing the National Institutes of Standards and Technology diffusion phantom in order to ensure that the measurements from diffusion MRI are stable(phantom)

Online Supplemental Method 2: Plasma NfL sampling methodology

Plasma NfL was quantified in a sub-cohort of participants from HANDLS from visits v_1 (2004-2009), v_2 (2009-2013) and v_3 (2013-2018), from which we extracted data from only v_1 and v_2 for our present study. This sub-sample included participants from the HANDLS SCAN, an ancillary neuroimaging sub-study, (n=238)(Waldstein et al., 2017) This sub-study of the HANDLS cohort excluded participants with a history of dementia, stroke, transient ischemic attack, and carotid endarterectomy, MRI contraindications, terminal illness, HIV positivity or other neurological disorders (Waldstein et al., 2017). All HANDLS SCAN participants included in this sub-study had donated plasma samples at three different visits except for one participant that had samples from only 2 of 3 visits. In addition, we also included participants (n=463; 1389 samples) that donated plasma samples at v_1, v_2 and v_3, who were HIV negative, had complete cognitive tests [Trailmaking test, part A (TRAILS A) and Digits Span-Forward (DS-F)[at v_1 and v_2, Centers of Epidemiologic Studies-Depression (CES-D) scores at all 3 visits and with no history of HIV, stroke, transient ischemic attack, dementia, epilepsy, Parkinson's disease or brain cancer. Participants (n=3) were also included who had plasma samples available from v_1, v_2 and v_3, who also had genome wide DNA methylation data at v_1(Beydoun et al., 2019a; Beydoun et al., 2020; Tajuddin et al., 2019). These participants had the exclusions listed above. Thus, overall, N=694 HANDLS participants had plasma NfL data at v_1 ; N=709 at v_2 and N=707.

Online Supplemental Method 3: Mixed-effects linear regression models and empirical Bayes estimation

The main multiple mixed-effects regression models can be summarized as follows:

	Multi-level models vs. **Composite models**	
Eq.		
1.1-1.4	$Y_{ij} = \pi_{0i} + \pi_{1i} Time_{ij} + \varepsilon_{ij}$	$\pi_{0i} = \gamma_{00} + \gamma_{0a} X_{aij} + \sum_{k=1}^{l} \gamma_{0k} Z_{ik} + \zeta_{0i}$
		$\pi_{1i} = \gamma_{10} + \gamma_{1a} X_{aij} + \sum_{m=1}^{n} \gamma_{1m} Z_{im} + \zeta_{1i}$
		$Y_{ij} = \gamma_{00} + \gamma_{0a} X_{aij} + \sum_{k=1}^{l} \gamma_{0k} Z_{ik} + \gamma_{10} Time_{ij} + \gamma_{1a} X_{aij} Time_{ij} + \sum_{m=1}^{n} \gamma_{1m} Z_{im} Time_{ij} + (\zeta_{0i} + \zeta_{1i} Time_{ij} + \varepsilon_{ij})$

Where Y_{ij} is the outcome (plasma NfL, Log_e transformed) for each individual "i" and visit "j"; π_{0i} is the level-1 intercept for individual i; π_{1i} is the level-1 slope for individual i; γ_{00} is the level-2 intercept of the random intercept π_{0i} ; γ_{10} is the level-2 intercept of the slope π_{1i} ; Z_{ik} is a vector of fixed covariates for each individual *i* that are used to predict level-1 intercepts and slopes and included baseline age (Age_{base}) among other covariates. $X_{ija,}$ represents the main predictor variables. In this case, all predictor variables were socio-demographic and used for prediction. ζ_{0i} and ζ_{1i} are level-2 disturbances; ε_{ij} is the within-person level-1 disturbance. Main effect of TIME (γ_{1a}) and interactions with socio-demographic factors (γ_{1a}) along with random effects ζ_{1i} were used to estimate each individual slope π_{1i} , also known as the empirical bayes estimator. The time interval model is described in details in this methodological paper.(Blackwell et al., 2006) Since time is measured as year elapsed since visit 1 up till visit 2, the interpretation of π_{1i} is the predicted individual-level annual rate of change in the outcome Y_{ij}, between visits 1 and 2. This empirical bayes estimator of slope was used to examine association between annual rates of change in NfL (Log_e transformed) vs. brain MRI markers. Below are the results of the mixed effects regression models for the plasma NfL exposure:

Table III.1. Mixed-effects linear regression model for plasma NfL (Log_e transformed) over time, with random intercept and slope and fixed effects for v1 age, sex, race, and poverty status interacted with TIME.

	NfL (n=729, k=1.9)
Intercept (γ_{00} ±SE)	+2.087789±0.0301934***
Time (γ_{10} ±SE)	+0.0367367±0.0069329***
Age(v_1) γ_{01}±SE	+0.0260676±0.0018511***
Age(v_1)×Time, γ_{11}±SE	+0.0005684±0.0004078
Sex (0=Female, 1=Male), γ_{02}±SE	+0.0944587±0.0334616**
Sex×Time, γ_{12}±SE	+0.0080145±0.007381
Race (0=Whites, 1=AA), γ_{03}±SE	-0.1836598±0.0333263***
Race×Time, γ_{13}±SE	+0.0075765±0.0074284
Poverty (0=Below, 1=Above), γ_{04}±SE	+0.0373991± 0.036728
Poverty×Time, γ_{14}±SE	0.0044728±0.0080016
Var (ζ_{0i})	+0.1672103±0.0124954
Var (ζ_{1i})	+0.0062101±0.0009051
Var (ε_{ij})	+0.0249631±0.007274

***p<0.001; **P<0.010; *p<0.05

The empirical bayes estimator for annual rate of change in NfL, Log_e transformed, can be summarized as follows:

$\gamma_{10} + \gamma_{11}\times$ Age $+ \gamma_{12}\times$ Sex $+ \gamma_{13}\times$ Race $+ \gamma_{14}\times$ Poverty $+ \zeta_{1i}$

Figure III.1 Baseline (v1), follow-up(v2) and annual rates of change in NfL scatter plot

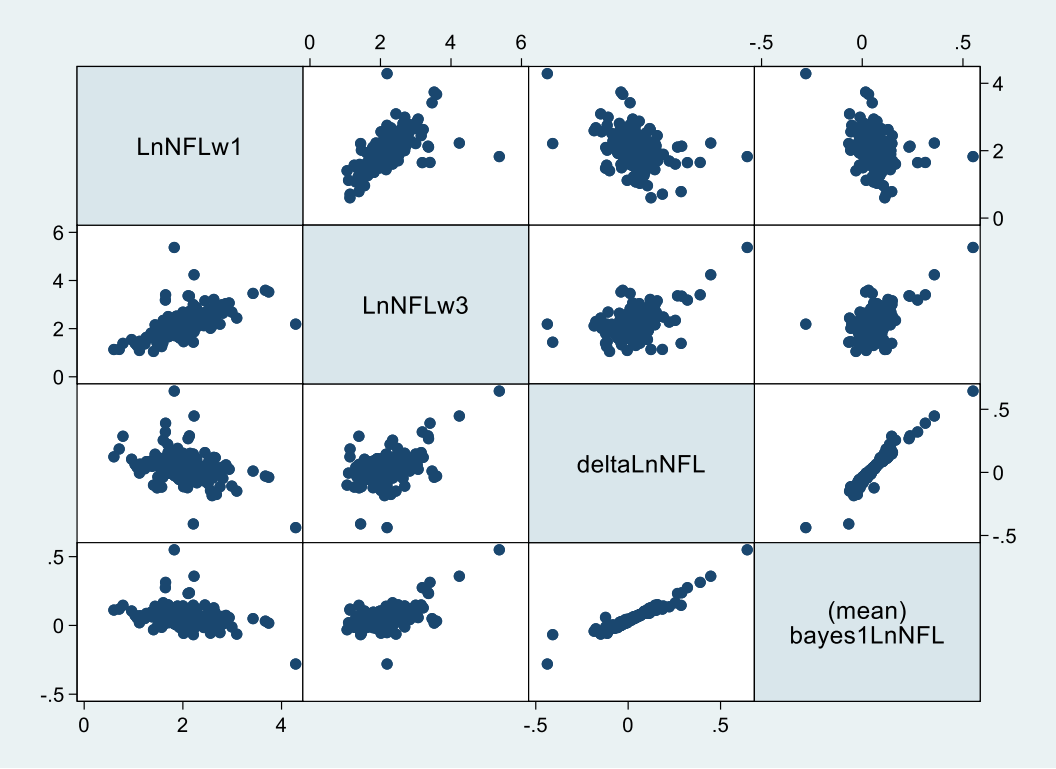

Abbreviations: NfL_{v1}=Plasma NfL (Log_e transformed) at visit 1 (HANDLS wave 1); NfLv2= Plasma NfL (Log_e transformed) at visit 2 (HANDLS wave 3); deltaNfL=Observed annual rate of change in Loge transformed NfL between visits 1 and 2; bayes1NfL=Empirical bayes estimator of annual rate of change in Loge transformed plasma NfL.

Supplemental Method 4: Additional covariates, LASSO regression and multiple imputations

A. Additional covariates:

A.1. Socio-demographic

Additional socio-demographic confounders included educational attainment (0 ≤ High School (HS); 1 = HS and 2 ≥ HS), the Wide Range Achievement Test (WRAT) letter and word reading subtotal scores to measure literacy, and marital status (1=married, 0=not married) (Beydoun et al., 2018).

A.2. Lifestyle

Smoking and drug use

Current use of opiates, marijuana or cocaine ("current" *vs*. "never or former") and smoking status ("current" vs. "never or former") were considered.

Adiposity measures
Measured body mass index (BMI, kg/m^2), waist circumference, and waist-hip-ratio were considered among potential confounders.

Healthy Eating Index 2010-
The Healthy Eating Index (HEI-2010) total score, based on two 24-hr recalls administered at baseline, was used as a measure of overall dietary quality. See steps for calculating HEI-2010 at http://appliedresearch.cancer.gov/tools/hei/tools.html and http://handls.nih.gov/06Coll-dataDoc.html.

Dietary Approaches to Stop Hypertension (DASH)

DASH diet adherence score, based on eight nutrients, was determined for each participant using the formula reported by Mellen *et al*.(Mellen et al.). The nine target nutrients were: total fat, saturated fat, protein, fiber, cholesterol, sodium, calcium, magnesium, and potassium. Micronutrient goals were expressed per 1000 kcal. The total DASH score was generated by the sum of all nutrient targets met. If the participant achieved the DASH target for a nutrient, a value of one was assigned, and if an intermediate target for a nutrient was achieved, a value of 0.5 was assigned. A value of zero was assigned if neither target was met. The maximum DASH score was nine; individuals meeting approximately half of the DASH targets (DASH score = 4.5) were considered DASH adherent (Mellen et al.).

Mean Adequacy Ratio (MAR)
Diet quality was also assessed using Nutrient Adequacy Ratio (NAR) and Mean Adequacy Ratio (MAR) scores(Fanelli Kuczmarski et al., 2013; Murphy et al., 2006). NAR score was determined by taking each participant's daily intake of a nutrient divided by the Recommended Dietary Allowance (RDA) for that nutrient. NAR scores were determined for 17 micronutrients: vitamins A, C, D, E, B_6, B_{12}, folate, iron, thiamin, riboflavin, niacin, copper, zinc, calcium, magnesium, phosphorus, and selenium. The RDA was adjusted for participants' ages and sexes and vitamin C was adjusted for smokers(Murakami et al., 2019). The NAR score was converted into a percent with values exceeding 100 truncated to 100. MAR scores were calculated by averaging the NAR scores: MAR= (∑NAR scores)/17(Fanelli Kuczmarski et al., 2018). NAR and MAR were calculated separately for each daily-intake and then averaged. MAR scores, based on food intakes only, were used as the nutrient-based diet quality variable.

Depressive symptoms
Depressive symptoms were operationalized using the CES-D at baseline and follow-up. The 20-item CES-D is a self-reported symptom rating scale assessing affective and depressed mood.(Radloff, 1977) A score of ≥16 on the CES-D is reflective of elevated depressive symptoms (EDS), (Ramos et al., 2004) and predicts clinical depression based on the Diagnostic and Statistical Manual, fourth edition (DSM-IV) criteria.(Myers and Weissman, 1980) Four CES-D sub-domains exhibiting an invariant factor structure between The National Health and Nutrition Examination Survey I and pilot HANDLS data (Nguyen et al., 2004) were computed. We tested our hypotheses using total and domain-specific CES-D scores: **(1)** Somatic complaints; **(2)** Depressive affect; **(3)** Positive affect and **(4)** Interpersonal problems.(Nguyen et al., 2004)

A.3. Health-related

Baseline chronic conditions included self-reported history measurement, biomarker-based measurement, and medication-based measurement, of type 2 diabetes, hypertension, dyslipidemia, cardiovascular disease, and inflammatory disease. Dyslipidemia was based on a combination of self-report, HDL, total cholesterol, triglyceride criteria, and statin use. Similarly, type 2 diabetes was determined using a combination of self-report, serum glucose criteria and medication. The same was conducted for hypertension. Additionally, a composite of cardiovascular

disease history was added in which self-reported stroke, congestive heart failure, non-fatal myocardial infarction or atrial fibrillation combined into a yes/no variable. Similarly, inflammatory disease was a binary composite of multiple sclerosis, systemic lupus, gout, rheumatoid arthritis, psoriasis, Thyroid disorder and Crohn's disease. The use of NSAIDs (prescription and over the counter) and statins over the past two weeks were considered separately as potential covariates.

A.4. Other biomarkers

All laboratory tests selected for this study were done at Quest Diagnostics, Chantilly, VA.

Serum cholesterol and atherogenic indices

Total cholesterol (TC), High density lipoprotein-cholesterol (HDL-C) and Triacylglycerols (TA) were assessed using a spectrophotometer (Olympus 5400). Low density lipoprotein-cholesterol (LDL-C) was calculated as TC-(HDL-C+TA/5) and directly measured in a sub-sample (N=236) using a spectrophotometer (Olympus 5400). The correlation between those with baseline calculated LDL-C and those with measured LDL-C was r~0.95. From these calculations, two relative measures were obtained, namely TC: HDL-C and LDL-C: HDL-C ratios. These were termed "atherogenic indices" and have been previously studied in relation to various cardiovascular outcomes that found them to be positively associated with measures of atherosclerosis and coronary heart disease. (Hisamatsu et al., 2014; Manickam et al., 2011; Nair et al., 2009)

Serum uric acid (SUA)

SUA measurements are useful in the diagnosis and treatment of renal and metabolic disorders, including renal failure, gout, leukemia, psoriasis, starvation or other wasting conditions, as well as in patients receiving cytotoxic drugs. Using 1 ml of fasting blood serum, uric acid was measured using a standard spectrophotometry method. The reference range for adult men is 4.0-8.0 mg/dL, whereas for women the range is 2.5-7.0 mg/dL. (http://www.questdiagnostics.com/testcenter/TestDetail.action?ntc=905) Other reference ranges were also recently suggested and depend on the menopausal status of women. Those reference ranges are based on predictive value for gout outcomes among healthy individuals and do not necessarily predict other pathologies. Thus, based on recent research evidence, a "normal" SUA value is suggested to be <6.0 mg/dL for all healthy adult individuals.

Serum albumin

Using 0.5-1 mL samples of plasma prepared with heparin and refrigerated for up to 30 days, albumin was measured with spectrophotometry, with an expected reference range of 3.6-5.1 g/dL(Beydoun et al., 2016b; Beydoun et al., 2019b).

High sensitivity C-reactive protein (CRP)

High sensitivity CRP (hs-CRP) was analyzed with an immunoturbidimeter (Siemens/Behring Nephelometer II), using 0.5-1 mL of plasma. A range of 1-10 mg/dL indicates average to high cardiovascular risk and >10 mg/dL suggests an infection or a chronic inflammation.

Serum creatinine

Using participant fasting blood specimens, baseline serum creatinine was measured at the National Institute on Aging, Clinical Research Branch Core Laboratory, using a modified kinetic Jaffe method (CREA method, Dade Dimension X-Pand Clinical Chemistry System, Siemens Healthcare Diagnostics Inc., Newark, DE) for a small group of participants (n=88). However, a majority of participants (n=1,528) had baseline serum creatinine analyzed at Quest Diagnostics, Inc. by isotope dilution mass spectrometry (IDMS) (Olympus America Inc., Melville, NY) and standardized to the reference laboratory, Cleveland Clinic. While inter-assay coefficients of variation (CV) for this sample could not be calculated due to the use of only one or the other measurement of creatinine at baseline, only intra-assay CVs (mean/SD) could be estimated. These were 0.192 and 0.187 for the CREA and the IDMS methods, respectively.

HbA1c

Glycated hemoglobin is derived from the nonenzymatic addition of glucose to amino groups of hemoglobin. HbA1c is a specific glycated hemoglobin that results from the attachment of glucose to the N-terminal valine of the hemoglobin b-chain. Numerous assays were subsequently developed to measure glycated hemoglobins. The principle of all methods is to separate the glycated and nonglycated forms of hemoglobin(Beydoun et al., 2016a). This can be accomplished based on differences in charge (usually by HPLC) or structure (usually immunoassays or boronate affinity chromatography). In this study, HPLC was used (Quest diagnostics).

White blood cell inflammatory markers

Fasting blood samples were collected from participants at baseline and follow-up to determine total white blood cell count (K/mm^3), using electronic Cell Sizing, counting, cytometry, and microscopy. (http://www.questdiagnostics.com/testcenter/TestDetail.action?ntc=7064).

Serum 25-hydroxyvitamin D, folate and cobalamin

Participants were asked to fast for ≥8 hours prior to the MRV visits, and serum specimens in volumes of 2 mL were collected and frozen at −80°C. Similar procedures were adopted for serum folate and cobalamin, both measured using chemiluminescence immunoassay (Siemens Centaur) by Quest Diagnostics, Chantilly, VA (Diagnostics; Wolters et al., 2005), and previously validated against other automated methods with coefficient of variation (CV) < 10% (Ispir et al., 2015; Owen and Roberts, 2003).

25(OH)D were measured using slightly revised methodologies between v_1 and v_2. In this study, only the v_1 measure was used. At v_1, total levels of serum 25(OH)D (in ng/ml; D_2 and D_3) were measured using tandem mass spectrometry (interassay CV, 8.6%) at Massachusetts General Hospital for less than 60 days later, as recommended for frozen samples (Powe et al., 2013). Blood samples drawn at examination were stored at −80°C.

Dietary and supplemental intakes of vitamin D, folate and cobalamin were shown to moderately correlate with their corresponding serum biomarkers in HANDLS and national surveys (Beydoun et al., 2010a; Beydoun et al., 2018; Beydoun et al., 2010b).

Hemoglobin and other hematological measures

Hemoglobin (Hb)

Similarly, using electronic cell sizing/cytometry/microscopy, Hb was assayed from a sample of 1 ml of blood drawn from participants after an overnight fast, and refrigerated up to 6 days (Quest diagnostics).

Other hematological markers

Ferritin: Ferritin is decreased in iron deficiency anemia and increases with iron overload. It is measured with immunoassay with reference ranges of 20-380 ng/mL among men and 10-232 ng/mL among women.(Diagnostics)

Erythrocyte Sedimentation Rate (ESR): Using 5 mL of refrigerated whole blood stored in lavender top EDTA tubes, the ESR was tested within 24 hr of blood draw. This test used automated modified Westergren photochemical capillary-stopped flow kinetic analysis.(Diagnostics; Larsson and Hansson, 2004) The Mayo Clinic reports a reference of 0-22 mm/hr for men and 0-29 mm/hr for women(Mayo Clinic, 2017) and is considered a proxy measure for serum fibrinogen.(Yin et al., 2017)

Serum iron: 0.5-1 mL of fasting serum was collected, transported at room temperature (with heparin added) and refrigerated or frozen subsequently. Serum iron was measured with spectrophotometry, (Diagnostics; Samarina and Proskurnin, 2015) with reference ranges for men aged ≥30y set at 50-180 µg/dL, and for women: 20-49y (40-190 µg /dL) and 50+y(45-160 µg /dL). (Diagnostics)

Mean Corpuscular Volume (MCV): Also known as erythrocyte mean corpuscular volume, MCV is measured using standard electronic cell sizing/counting/cytometry/microscopy. Similar to other hemogram measures (e.g. ESR), a microtainer 1 mL whole blood in an EDTA (lavender-top) tube was transported at room temperature to the laboratory facility.(Diagnostics)

Mean Cell Hemoglobin (MCH): The hematologic index MCH was calculated as follows: MCH = Hb/RBC.

Red Cell Distribution Width (RDW): RDW was calculated by automated Coulter DXH 800 hematology analyzer as part of peripheral complete blood count (Beckman Coulter, Brea, CA). The analyzer underwent regular calibration every three months and quality control procedures (Diagnostics). Clinical analysis typically includes two RDW measurements, i.e. the RDW-CV (unit: %), which we adopted in this study, and the RDW-Standard Deviation (SD, unit: fL) from which RDW-CV is obtained. RDW-CV=RDW-SD×100/MCV, MCV being the mean cell volume. RDW-CV's normal range is 11.0 - 15.0%, and it depends on width of the distribution (normal range: 40-55 fL) curve and MCV (techs, 2019).

Other measures and their methods of quantification are listed below:

Variable	HANDLS Variable Label	Description	Source
ALP	Alkaline phosphatase (U/L)	This liver enzyme was measured at Quest diagnostics using spectrophotometry. URL: https://testdirectory.questdiagnostics.com/test/test-detail/234/alkalinephosphatase?cc=MASTER	https://handls.nih.gov/pubs/2021-Beydoun-AffectiveDisorders-282-858.pdf
ALT	ALT [SGPT] (U/L)	Beckman Coulter AU5400®	https://www.ncbi.nlm.nih.gov/pmc/articles/PMC5882538/
Amylase	Amylase (U/L)	Spectrophotometry Reference Range(s) 21-101 U/L	https://testdirectory.questdiagnostics.com/test/test-detail/243/amylase?cc=MASTER
AST	AST [SGOT] (U/L)	Beckman Coulter AU5400®	https://www.ncbi.nlm.nih.gov/pmc/articles/PMC5882538/
BiliDir	Direct [conjugated] bilirubin (mg/dL)	Spectrophotometry	https://testdirectory.questdiagnostics.com/test/test-detail/287/bilirubin-total?cc=MASTER
BiliTot	Total bilirubin (mg/dL)	Spectrophotometry	https://testdirectory.questdiagnostics.com/test/test-detail/287/bilirubin-total?cc=MASTER
BUN	Blood urea nitrogen (mg/dL)	Beckman Coulter AU5400®	https://www.ncbi.nlm.nih.gov/pmc/articles/PMC5882538/
Calcium	Calcium (mg/dL)	Spectrophotometry	https://testdirectory.questdiagnostics.com/test/test-detail/303/calcium?cc=MASTER
Cl	Chloride (mmol/L)	Ion Selective Electrode (ISE) Reference Range(s) 98-110 mmol/L	https://testdirectory.questdiagnostics.com/test/test-detail/330/chloride?cc=MASTER

CO2	Carbon dioxide (mmol/L)	Spectrophotometry Reference Range(s) 20-32 mmol/L	https://testdirectory.questdiagnostics.com/test/test-detail/310/carbon-dioxide?cc=MASTER
EosinPct	WBC Eosinophil (%)	Electronic Counting and Sizing • Cytometry • Microscopy	https://testdirectory.questdiagnostics.com/test/test-detail/425/eosinophil-count-blood?cc=MASTER
FeSat	Iron saturation (%)	1.1.1 Spectrophotometry 1.1.2 1.1.3 Minimum Volume: 0.5 mL 1.1.4 Transport Temperature: Room temperature 1.1.5 Specimen Stability • Room temperature: 6 days • Refrigerated: 7 days • Frozen: 28 days	https://testdirectory.questdiagnostics.com/test/test-detail/7573/iron-total-and-total-iron-binding-capacity?cc=MASTER
GGT	Gamma glutamyl transferase (U/L)	Spectrophotometry 1.1.6 Preferred Specimen(s): 1 mL serum 1.1.7 Minimum Volume: 0.5 mL Specimen Stability • Room temperature: 7 days • Refrigerated: 7 days • Frozen: 28 days	https://testdirectory.questdiagnostics.com/test/test-detail/482/gamma-glutamyl-transferase-ggt?cc=MASTER
HBV	Hepatitis B surface antigen	Immunoassay (IA) 1.1.8 Minimum Volume: 1 mL 1.1.9 Transport Temperature: Room temperature 1.1.10 Specimen Stability • Room temperature: 7 days • Refrigerated: 14 days • Frozen: 30 days	https://testdirectory.questdiagnostics.com/test/test-detail/498/hepatitis-b-surface-antigen-with-reflex-confirmation?cc=MASTER
Hct	Hematocrit (%)	Electronic Cell, Sizing/Cytometry/Microscopy 1.1.11 Minimum Volume: Microtainer: 0.5 mL • EDTA (lavender-top) tube: 1 mL 1.1.12 1.1.13 Transport Temperature: Room temperature 1.1.14 1.1.15 Specimen Stability • Room temperature: 48 hours • Refrigerated: 48 hours (may cause platelet clumping) • Frozen: Unstable	https://testdirectory.questdiagnostics.com/test/test-detail/509/hematocrit?cc=MASTER

HCV	Hepatitis C	Immunoassay (IA) 1.1.16 Minimum Volume: 3 mL 1.1.17 Transport Temperature: Room temperature 1.1.18 Specimen Stability • Room temperature: 72 hours • Refrigerated: 14 days • Frozen: 30 days	https://testdirectory.questdiagnostics.com/test/test-detail/8472/hepatitis-c-antibody-with-reflex-to-hcv-rna-quantitative-real-time-pcr?cc=MASTER
Insulin	Serum insulin (uIU/mL)	Immunoassay (IA) 1.1.19 Reference Range(s) ≤19.6 uIU/mL 1.1.20 Minimum Volume: 0.5 mL 1.1.21 Transport Temperature: Refrigerated (cold packs) 1.1.22 Specimen Stability • Room temperature: 8 hours • Refrigerated: 7 days • Frozen: 28 days	https://testdirectory.questdiagnostics.com/test/test-detail/561/insulin?cc=MASTER
K	Potassium (mmol/L)	Beckman Coulter AU5400®	https://www.ncbi.nlm.nih.gov/pmc/articles/PMC5882538/
LDH	Lactate dehydrogenase (U/L)	Beckman Coulter AU5400®	https://www.ncbi.nlm.nih.gov/pmc/articles/PMC5882538/
MCH	Mean cell hemoglobin (pg)	The hematologic index MCH was calculated as follows: MCH = Hb/RBC.	
MCV	Mean cell volume (fL)	Reference range: 80.0 - 100.0 fL	https://www.radc.rush.edu/docs/var/detail.htm?category=Blood%20Measures&subcategory=Routine%20laboratory%20tests&variable=mcv
Mg	Magnesium (mg/dL)	Spectrophotometry 1.1.23 Reference Range(s): 1.5-2.5 mg/dL 1.1.24 Minimum Volume: 0.5 mL 1.1.25 Transport Temperature: Room temperature 1.1.26 1.1.27 Specimen Stability • Serum and plasma • Room temperature: 7 days • Refrigerated: 7 days • Frozen: 28 days	https://testdirectory.questdiagnostics.com/test/test-detail/622/magnesium?cc=MASTER

Na	Sodium (mmol/L)	Ion Selective Electrode (ISE) 1.1.28 **Reference Range(s):** 135-146 mmol/L 1.1.29 **Minimum Volume:** 0.5 mL 1.1.30 **Transport Temperature:** Room temperature	https://testdirectory.questdiagnostics.com/test/test-detail/836/sodium?cc=MASTER
Phosphate	Phosphate (mg/dL)	Spectrophotometry 1.1.31 **Minimum Volume:** 0.5 mL 1.1.32 **Transport Temperature:** Room temperature 1.1.33 **Specimen Stability** • Room temperature: 72 hours • Refrigerated: 7 days • Frozen: 28 days	https://testdirectory.questdiagnostics.com/test/test-detail/718/phosphate-as-phosphorus?cc=MASTER
Platelets	Platelet count (10^9/L)	Electronic Cell Sizing/Counting/Cytometry/Microscopy Reference Range(s) ≤3 Days 150-450 Thousand/µL 4 Days-6 Months 150-400 Thousand/µL >6 Months 140-400 Thousand/µL 1.1.34 **Minimum Volume:** Microtainer 0.5 mL 1 mL whole blood EDTA (lavender-top) tube 1.1.35 1.1.36 **Transport Temperature:** Room temperature - do not refrigerate 1.1.37 1.1.38 **Specimen Stability** • Room temperature: 48 hours • Refrigerated: Not provided • Frozen: Not provided	https://testdirectory.questdiagnostics.com/test/test-detail/723/platelet-count-edta?cc=MASTER
RPR	RPR screen	Flocculation 1.1.39 **Reference Range(s):** Non-Reactive 1.1.40 **Preferred Specimen(s):** 1 mL serum 1.1.41 1.1.42 **Specimen Stability** • Room temperature: 4 days • Refrigerated: 7 days • Frozen: 30 days	https://testdirectory.questdiagnostics.com/test/test-detail/799/rpr-monitor-with-reflex-to-titer?cc=MASTER

T3uptake	T3 uptake (%)	Immunoassay (IA) 1.1.43 Reference Range(s): 22-35 % 1.1.44 Minimum Volume: 0.5 mL 1.1.45 Transport Temperature: Room temperature 1.1.46 Specimen Stability • Room temperature: 7 days • Refrigerated: 10 days • Frozen: 28 days	https://testdirectory.questdiagnostics.com/test/test-detail/861/t3-uptake?cc=MASTER
T4Feee	T4 free n(g/dL)	Immunoassay (IA) 1.1.47 Minimum Volume: 0.3 mL 1.1.48 Transport Temperature: Room temperature 1.1.49 Specimen Stability • Room temperature: 7 days • Refrigerated: 7 days • Frozen: 28 days	https://testdirectory.questdiagnostics.com/test/test-detail/866/t4-free-ft4?cc=MASTER
T4tot	T4 [thyroxine] total mcg/dL	Immunoassay (IA) 1.1.50 Minimum Volume: 0.5 mL 1.1.51 Transport Temperature: Room temperature 1.1.52 Specimen Stability • Room temperature: 7 days • Refrigerated: 7 days • Frozen: 28 days	https://testdirectory.questdiagnostics.com/test/test-detail/867/t4-thyroxine-total?cc=MASTER
TIBC	Total iron binding capacity mcg/dL	Spectrophotometry 1.1.53 Minimum Volume: 0.5 mL 1.1.54 Transport Temperature: Room temperature 1.1.55 Specimen Stability • Room temperature: 6 days • Refrigerated: 7 days • Frozen: 28 days	https://testdirectory.questdiagnostics.com/test/test-detail/7573/iron-total-and-total-iron-binding-capacity?cc=MASTER
Triglyc	Triglyceride (mg/dL)	Spectrophotometry Reference Range(s): <150 mg/dL	https://testdirectory.questdiagnostics.com/test/test-detail/896/triglycerides?cc=MASTER

		1.1.56 Minimum Volume: 0.5 mL 1.1.57 Transport Temperature: Room temperature 1.1.58 Specimen Stability • Serum and plasma • Room temperature: 5 days • Refrigerated: 7 days • Frozen: 28 days	
TSH	Thyroid-stimulating hormone (mIU/L)	Immunoassay (IA) 1.1.59 Minimum Volume: 0.7 mL 1.1.60 Transport Temperature: Room temperature 1.1.61 Specimen Stability • Room temperature: 7 days • Refrigerated: 7 days • Frozen: 28 days	https://testdirectory.questdiagnostics.com/test/test-detail/899/tsh?cc=MASTER
UpH	Urine pH	pH Meter 1.1.62 Reference Range(s): 4.6-8.0 1.1.63 Minimum Volume: 10 mL 1.1.64 Transport Temperature: Room temperature	https://testdirectory.questdiagnostics.com/test/test-detail/8452/ph-urine?cc=MASTER
USpecGrav	Urine specific gravity	Reagent Impregnated Strips 1.1.65 Reference Range(s): 1.001-1.035 1.1.66 1.1.67 Minimum Volume: Preserved: 1 mL 1.1.68 Transport Temperature: Preserved: Room temperature 1.1.69	https://testdirectory.questdiagnostics.com/test/test-detail/3190/specific-gravity-urine?cc=MASTER
Eosinophils	WBC Eosinophil count (10^9/L)	Methodology Electronic Counting and Sizing • Cytometry • Microscopy	https://testdirectory.questdiagnostics.com/test/test-detail/425/eosinophil-count-blood?cc=MASTER
Lipase	Lipase (U/L)	Spectrophotometry; Reference Range(s) 7-60 U/L	https://testdirectory.questdiagnostics.com/test/test-detail/606/lipase?cc=MASTER
UCreatinine	Urine creatinine	Colorimetric (C) • Kinetic	https://testdirectory.questdiagnostics.com/test/test-detail/8459/creatinine-random-urine?cc=MASTER

		1.1.70 Preferred Specimen(s): 10 mL random urine, no preservative 1.1.71 Minimum Volume: 0.5 mL 1.1.72 Transport Temperature: Room temperature 1.1.73 Specimen Stability • Room temperature: 7 days • Refrigerated: 7 days • Frozen: 28 days	
UMicroAlb	Urine microalbumin	Immunoturbimetric assay (Kamiya Biomedical Co., Seattle, WA). CKD was defined as an estimated glomerular filtration rate (eGFR) <60 mL/min per 1.73 m2 calculated using the CKD Epidemiology Collaboration creatinine-based equation	immunoturbimetric assay (Kamiya Biomedical Co., Seattle, WA). CKD was defined as an estimated glomerular filtration rate (eGFR) <60 mL/min per 1.73 m2 calculated using the CKD Epidemiology Collaboration creatinine-based equation

B. Least absolute shrinkage and selection operator (LASSO) regression procedure

In order to select the appropriate set of predictive models for NfL, we used a statistical learning method for variable selection known as adaptive LASSO and compared it to cross-validation LASSO (cvLASSO) and lowest BIC LASSO. Socio-demographic variables, (age, sex, race/ethnicity, poverty status) were force entered as fixed terms into all models. The LASSO then selected among the other covariates listed above as variables that should be retained. Covariates were imputed using chained equations (5 imputations, 10 iterations), accounting for their level of measurement. Socio-demographic factors were entered into all the chained equations. Continuous covariates were entered as outcomes in a series of linear regression models, while binary and categorical variables were entered into a series of multinomial logit regression models.

LASSO is a covariate selection methodology that is superior to both generalized linear models without covariate selection as well as the usually applied stepwise or backward elimination process.(Zou, 2006) In fact, stepwise selection is often trapped into a local optimal solution rather than the global optimal solution and backward elimination can be time-consuming given the large number of variables in the full model.(Zou, 2006) These methods often ignore stochastic errors or uncertainty incurred during variable selection, with the LASSO estimate being defined as:

$$\beta(\text{lasso}) = \arg min_{\beta} \| y - \sum_{j=1}^{p} x_j \beta_j \|^2 + \lambda \sum_{j=1}^{p} |\beta_j|$$

with λ being a nonnegative regularization parameter.(Zou, 2006) The second term of the equation termed the "l1 penalty" is a key portion of this equation that ensures the success of the lasso method of covariate selection. This method was shown to discover the right sparse representation of the model, given certain conditions. Nevertheless, this method can produce biased estimates for larger coefficients. Thus, there a number of scenarios whereby the LASSO can yield inconsistent results. Recent methods have shown that an adaptive version of the LASSO gave more consistent findings, particularly when compared with the nonnegative garotte, another popular variable selection technique.

In our modeling approach, we used this convex optimization technique with l_1 constraint known as adaptive LASSO as one of three methods to select the final linear regression models. The model is trained on a random half sample of the total population (first imputation out of 5) and validated against the other half sample to check robustness of findings, by comparing R^2 between samples. One model was selected among the cvLASSO, adaptive LASSO or minBIC LASSO, depending on how close the R^2 are between half-samples. This parsimonious model selected for NfL exposures, Log_e transformed, (measured at v_1 and v_2) as 2 potential outcomes is then run on the entire population and a backward elimination process is carried out to keep only significant covariates at type I error

= 0.10. Thus, the selected model through LASSO was used as a starting point for further backward elimination. Backward elimination was conducted on the imputed data for the entire sample, rather than the half sample for the first imputation.

In our analysis, the following LASSO models were selected, and the final model included is shown also in this Table.

Table IV.1. Results of LASSO selection models and backward elimination

	Selected covariates[1]			
	cvLASSO	**Min BIC LASSO**	**Adaptive LASSO**	**Reduced model**
NfL (v1)	Age, Race, BMI, current drug use, insulin, phosphate, Chlorine, CO2, poverty status, urinary specific gravity, creatinine, sex, potassium, lipase, platelets, education, self-rated health, Chol:HDL ratio, TIBC	Age, Race, Poverty Status, Sex	**Age, Race, BMI, current drug use, phosphate, CO2, Poverty status, urinary specific gravity, creatinine, Sex, lipase, platelets, education, Chol:HDL ratio, TIBC, albumin, HbA1C, self-rated health, 25(OH)D, HDL-cholesterol, glucose, LDL-cholesterol, ALT, LDH, Basophils as % total WBC, Blood urea nitrogen, Diabetes, amylase, TSH, hypertension, albumin:globulin ratio, CES-D total score, neutrophils, MCV, microalbumin**	**Age, Race, BMI, current drugs, poverty status, urinary specific gravity, creatinine, sex, albumin, self-rated health, 25(OH)D**
NfL (v2)	Age, Race, GGT, BMI, Creatinine, Chlorine, insulin, lipase, amylase, HbA1C, Poverty status, sex, self-rated health, NSAIDs, ALP, WHR, WBC, Neutrophils % total WBC, Urinary specific gravity, blood urea nitrogen, smoking, B12, self-rated health, RPR, CRP, HIV, hypertension	Age, Race, Poverty Status, Sex	**Age, Race, GGT, BMI, Creatinine, Chlroine, insulin, lipase, amylase, HbA1C, poverty status, sex, WHR, neutrophils as % WBC, urinary specific gravity, self-rated health, serum glucose, uric acid, eosinophils as % WBC, HDL-cholesterol, Diabetes, current drug sue, CES-D total score, ESR, LDH**	**Age, sex, race, poverty status, BMI, Creatinine, ALP, Urinary specific gravity, blood urea nitrogen, serum glucose, uric acid, eosinophils as % WBC, Diabetes**

Abbreviations: BIC=Bayesian information criterion; BMI=Body Mass Index; cv=cross-validation; CVD=Self-reported cardiovascular disease; LASSO= Least absolute shrinkage and selection operator; A full row of bolded sets of covariates indicates that the selection process is equivalent, and that backward elimination did not reduce the model further.

The final common set of covariates that were chosen using the reduced model for each exposure was:

NfL at v_1: Age, Race, BMI, current drugs, poverty status, urinary specific gravity, creatinine, sex, albumin, self-rated health, 25(OH)D

NfL at v_2: Age, sex, race, poverty status, BMI, Creatinine, ALP, Urinary specific gravity, blood urea nitrogen, serum glucose, uric acid, eosinophils as % WBC, Diabetes

From these, six models were constructed:

Model 1: Only socio-demographic

Model 2: Socio-demographic + BMI

Model 3: Socio-demographic +BMI + serum glucose+diabetes.

Model 4: Socio-demographic +BMI +kidney/liver disease markers (Creatinine, ALP, Urinary specific gravity, blood urea nitrogen, uric acid).

Model 5:Socio-demographic+BMI+inflammatory markers (25(OH)D, eosinophils as % WBC, albumin)

Model 6: Socio-demographic +BMI+lifestyle/health related factors (current drug use, self-rated health).

C. Full description of the modeling approach:

Using multiple imputed data (k=5 imputations), a sensitivity analysis (SA) adjusted for additional covariates, selected with a multi-step process detailed in **supplemental method 4**, that included machine learning, followed by backward elimination and finally selection of a common pool of covariates that were independent predictors of one of two exposures. The pool of covariates initially selected had exhibited associations with either NfL measures and/or cognitive outcomes in previous studies. Thus, the final modeling approach consisted of a minimally adjusted basic model i.e., **Model 1** conducted on the unimputed data. Subsequently, the SA was carried out on multiple imputed data, with the following modeling approach, running in a serial manner Models 2 through 6 described in **B**.

Supplemental References:

Beydoun, M.A., Beydoun, H.A., Mode, N., Dore, G.A., Canas, J.A., Eid, S.M., Zonderman, A.B., 2016a. Racial disparities in adult all-cause and cause-specific mortality among us adults: mediating and moderating factors. BMC Public Health 16(1), 1113.

Beydoun, M.A., Canas, J.A., Dore, G.A., Beydoun, H.A., Rostant, O.S., Fanelli-Kuczmarski, M.T., Evans, M.K., Zonderman, A.B., 2016b. Serum Uric Acid and Its Association with Longitudinal Cognitive Change Among Urban Adults. J Alzheimers Dis 52(4), 1415-1430.

Beydoun, M.A., Fanelli Kuczmarski, M.T., Beydoun, H.A., Shroff, M.R., Mason, M.A., Evans, M.K., Zonderman, A.B., 2010a. The sex-specific role of plasma folate in mediating the association of dietary quality with depressive symptoms. J Nutr 140(2), 338-347.
Beydoun, M.A., Hossain, S., Chitrala, K.N., Tajuddin, S.M., Beydoun, H.A., Evans, M.K., Zonderman, A.B., 2019a. Association between epigenetic age acceleration and depressive symptoms in a prospective cohort study of urban-dwelling adults. J Affect Disord 257, 64-73.
Beydoun, M.A., Hossain, S., Fanelli-Kuczmarski, M.T., Beydoun, H.A., Canas, J.A., Evans, M.K., Zonderman, A.B., 2018. Vitamin D Status and Intakes and Their Association With Cognitive Trajectory in a Longitudinal Study of Urban Adults. J Clin Endocrinol Metab 103(4), 1654-1668.
Beydoun, M.A., Obhi, H.K., Weiss, J., Canas, J.A., Beydoun, H.A., Evans, M.K., Zonderman, A.B., 2019b. Systemic inflammation is associated with depressive symptoms differentially by sex and race: a longitudinal study of urban adults. Mol Psychiatry.
Beydoun, M.A., Shaked, D., Tajuddin, S.M., Weiss, J., Evans, M.K., Zonderman, A.B., 2020. Accelerated epigenetic age and cognitive decline among urban-dwelling adults. Neurology 94(6), e613-e625.
Beydoun, M.A., Shroff, M.R., Beydoun, H.A., Zonderman, A.B., 2010b. Serum folate, vitamin B-12, and homocysteine and their association with depressive symptoms among U.S. adults. Psychosom Med 72(9), 862-873.
Blackwell, E., de Leon, C.F., Miller, G.E., 2006. Applying mixed regression models to the analysis of repeated-measures data in psychosomatic medicine. Psychosom Med 68(6), 870-878.
Diagnostics, Q., Ferritin. https://www.questdiagnostics.com/testcenter/TestDetail.action?ntc=457&searchString=8272. (Accessed May 13sth 2019).
Diagnostics, Q., Hemogram. https://www.questdiagnostics.com/testcenter/BUOrderInfo.action?tc=7008&labCode=DAL. (Accessed May 13sth 2019).
Diagnostics, Q., Iron, Total and Total Iron Binding Capacity. https://www.questdiagnostics.com/testcenter/BUOrderInfo.action?tc=7573&labCode=SEA. (Accessed May 13sth 2019).
Diagnostics, Q., Vitamin B-12 (cobalamin) and folate panel. https://testdirectory.questdiagnostics.com/test/test-detail/7065/vitamin-b12-cobalamin-and-folate-panel-serum?cc=MASTER. (Accessed October 21st 2019).
Doshi, J., Erus, G., Ou, Y., Gaonkar, B., Davatzikos, C., 2013. Multi-atlas skull-stripping. Acad Radiol 20(12), 1566-1576.
Doshi, J., Erus, G., Ou, Y., Resnick, S.M., Gur, R.C., Gur, R.E., Satterthwaite, T.D., Furth, S., Davatzikos, C., Alzheimer's Neuroimaging, I., 2016. MUSE: MUlti-atlas region Segmentation utilizing Ensembles of registration algorithms and parameters, and locally optimal atlas selection. Neuroimage 127, 186-195.
Fanelli Kuczmarski, M., Bodt, B.A., Stave Shupe, E., Zonderman, A.B., Evans, M.K., 2018. Dietary Patterns Associated with Lower 10-Year Atherosclerotic Cardiovascular Disease Risk among Urban African-American and White Adults Consuming Western Diets. Nutrients 10(2).
Fanelli Kuczmarski, M., Mason, M.A., Beydoun, M.A., Allegro, D., Zonderman, A.B., Evans, M.K., 2013. Dietary patterns and sarcopenia in an urban African American and White population in the United States. J Nutr Gerontol Geriatr 32(4), 291-316.

Gunter, J.L., Bernstein, M.A., Borowski, B.J., Ward, C.P., Britson, P.J., Felmlee, J.P., Schuff, N., Weiner, M., Jack, C.R., 2009. Measurement of MRI scanner performance with the ADNI phantom. Med Phys 36(6), 2193-2205.
Hisamatsu, T., Fujiyoshi, A., Miura, K., Ohkubo, T., Kadota, A., Kadowaki, S., Kadowaki, T., Yamamoto, T., Miyagawa, N., Zaid, M., Torii, S., Takashima, N., Murakami, Y., Okamura, T., Horie, M., Ueshima, H., Group, S.R., 2014. Lipoprotein particle profiles compared with standard lipids in association with coronary artery calcification in the general Japanese population. Atherosclerosis 236(2), 237-243.
Ispir, E., Serdar, M.A., Ozgurtas, T., Gulbahar, O., Akin, K.O., Yesildal, F., Kurt, I., 2015. Comparison of four automated serum vitamin B12 assays. Clin Chem Lab Med 53(8), 1205-1213.
Larsson, A., Hansson, L.O., 2004. Analysis of inflammatory response in human plasma samples by an automated multicapillary electrophoresis system. Clin Chem Lab Med 42(12), 1396-1400.
Li, C., Gore, J.C., Davatzikos, C., 2014. Multiplicative intrinsic component optimization (MICO) for MRI bias field estimation and tissue segmentation. Magn. Reson. Imaging 32(7), 913-923.
Manickam, P., Rathod, A., Panaich, S., Hari, P., Veeranna, V., Badheka, A., Jacob, S., Afonso, L., 2011. Comparative prognostic utility of conventional and novel lipid parameters for cardiovascular disease risk prediction: do novel lipid parameters offer an advantage? Journal of clinical lipidology 5(2), 82-90.
Mayo Clinic, 2017. Sed rate (erythrocyte sedimentation rate). https://www.mayoclinic.org/tests-procedures/sed-rate/about/pac-20384797. (Accessed May 10th 2019).
Mellen, P.B., Gao Sk Fau - Vitolins, M.Z., Vitolins Mz Fau - Goff, D.C., Jr., Goff, D.C., Jr., Deteriorating dietary habits among adults with hypertension: DASH dietary accordance, NHANES 1988-1994 and 1999-2004. (0003-9926 (Print)).
Mulkern, R.V., Forbes, P., Dewey, K., Osganian, S., Clark, M., Wong, S., Ramamurthy, U., Kun, L., Poussaint, T.Y., 2008. Establishment and results of a magnetic resonance quality assurance program for the pediatric brain tumor consortium. Acad Radiol 15(9), 1099-1110.
Murakami, K., Livingstone, M.B.E., Sasaki, S., 2019. Diet quality scores in relation to metabolic risk factors in Japanese adults: a cross-sectional analysis from the 2012 National Health and Nutrition Survey, Japan. Eur J Nutr 58(5), 2037-2050.
Murphy, S.P., Foote, J.A., Wilkens, L.R., Basiotis, P.P., Carlson, A., White, K.K., Yonemori, K.M., 2006. Simple measures of dietary variety are associated with improved dietary quality. Journal of the American Dietetic Association 106(3), 425-429.
Myers, J.K., Weissman, M.M., 1980. Use of a self-report symptom scale to detect depression in a community sample. Am J Psychiatry 137(9), 1081-1084.
Nair, D., Carrigan, T.P., Curtin, R.J., Popovic, Z.B., Kuzmiak, S., Schoenhagen, P., Flamm, S.D., Desai, M.Y., 2009. Association of total cholesterol/ high-density lipoprotein cholesterol ratio with proximal coronary atherosclerosis detected by multislice computed tomography. Preventive cardiology 12(1), 19-26.
Nguyen, H.T., Kitner-Triolo, M., Evans, M.K., Zonderman, A.B., 2004. Factorial invariance of the CES-D in low socioeconomic status African Americans compared with a nationally representative sample. Psychiatry Res 126(2), 177-187.
Owen, W.E., Roberts, W.L., 2003. Comparison of five automated serum and whole blood folate assays. Am J Clin Pathol 120(1), 121-126.
phantom, N.d.

Powe, C.E., Evans, M.K., Wenger, J., Zonderman, A.B., Berg, A.H., Nalls, M., Tamez, H., Zhang, D., Bhan, I., Karumanchi, S.A., Powe, N.R., Thadhani, R., 2013. Vitamin D-binding protein and vitamin D status of black Americans and white Americans. N Engl J Med 369(21), 1991-2000.
Radloff, L., 1977. The CES-D scale: a self-report depression scale for research in the general population. Applied Psychological Measurement 1(385-401).
Ramos, M.I., Allen, L.H., Haan, M.N., Green, R., Miller, J.W., 2004. Plasma folate concentrations are associated with depressive symptoms in elderly Latina women despite folic acid fortification. Am J Clin Nutr 80(4), 1024-1028.
Samarina, T., Proskurnin, M., 2015. Rapid assessment of iron in blood plasma and serum by spectrophotometry with cloud-point extraction. F1000Res 4, 623.
Tajuddin, S.M., Hernandez, D.G., Chen, B.H., Noren Hooten, N., Mode, N.A., Nalls, M.A., Singleton, A.B., Ejiogu, N., Chitrala, K.N., Zonderman, A.B., Evans, M.K., 2019. Novel age-associated DNA methylation changes and epigenetic age acceleration in middle-aged African Americans and whites. Clin Epigenetics 11(1), 119.
techs, O.l.c.e.f.c.l.a.m., 2019. Red Blood Cell Distribution Width (RDW): Definition and Calculation.
Waldstein, S.R., Dore, G.A., Davatzikos, C., Katzel, L.I., Gullapalli, R., Seliger, S.L., Kouo, T., Rosenberger, W.F., Erus, G., Evans, M.K., Zonderman, A.B., 2017. Differential Associations of Socioeconomic Status With Global Brain Volumes and White Matter Lesions in African American and White Adults: the HANDLS SCAN Study. Psychosom Med 79(3), 327-335.
Wolters, M., Hickstein, M., Flintermann, A., Tewes, U., Hahn, A., 2005. Cognitive performance in relation to vitamin status in healthy elderly German women-the effect of 6-month multivitamin supplementation. Prev Med 41(1), 253-259.
Yin, W., Xu, Z., Sheng, J., Xie, X., Zhang, C., 2017. Erythrocyte sedimentation rate and fibrinogen concentration of whole blood influences the cellular composition of platelet-rich plasma obtained from centrifugation methods. Exp Ther Med 14(3), 1909-1918.
Zou, H., 2006. The adaptive Lasso and it oracle properties. Journal of the American Statistical Association 101(476), 1418-1428.

Online Supplementary Results 1

Similarly, **Table S2** explores those same study characteristics distributions in the total population, across NfL exposure tertiles (i.e. Log_e transformed plasma NfL, at v_1 and v_2). Generally, baseline age was directly related to NfL tertiles, with a 11-12y difference in mean age between the lowest and uppermost tertile. Percent above poverty was more elevated in the uppermost tertile of NfL at v_1 vs. lowest tertile (83.1% vs. 56.7%), but not at v_2. In contrast, mean BMI was lower in the uppermost tertile of NfL at v_1 vs. the lowest tertile (30.9 vs. 27.6, $P_{trend}<0.01$), a relationship that remained significant after further adjustment for age, sex, race and poverty status. While several lifestyle, health-related and laboratory indices were either directly or inversely related to NfL tertile, only a few remained significant correlates after adjustment for age, sex, race and poverty status. Specifically, alkaline phosphatase was directly related to NfL tertile at v_2 with a mean of 83.0 in the uppermost tertile vs. 69.3 in the lowest ($P_{trend}<0.001$), while 25(OH)D was inversely related to NfL tertile at v_1, with a mean of 26.4 in the uppermost tertile vs. 18.5 in the lowest ($P_{trend}<0.001$). NfL tertile at v_1 was directly related to WMLV after adjustment for age, sex, race, poverty status and ICV ($P_{trend}<0.010$). All other bivariate associations between NfL tertiles and sMRI measures, including hippocampal volumes, were attenuated with addition of socio-demographic factors.

Table S1. ROIs included in the small ROI volumes analyses (Analysis A") and WMLV analysis C' : volcano plots and FSLEYES analyses[a]

SMALL ROI VOLUMES	SMALL ROI WMLV
3rd.Ventricle_volM2	**3rd.Ventricle_wmlM2**
4th.Ventricle_volM2	**4th.Ventricle_wmlM2**
Right.Accumbens.Area_volM2	**Right.Accumbens.Area_wmlM2**
Left.Accumbens.Area_volM2	**Left.Accumbens.Area_wmlM2**
Right.Amygdala_volM2	Right.Amygdala_wmlM2
Left.Amygdala_volM2	Left.Amygdala_wmlM2
Brain.Stem_volM2	**Brain.Stem_wmlM2**
Right.Caudate_volM2	**Right.Caudate_wmlM2**
Left.Caudate_volM2	**Left.Caudate_wmlM2**
Right.Cerebellum.Exterior_volM2	**Right.Cerebellum.Exterior_wmlM2**
Left.Cerebellum.Exterior_volM2	Left.Cerebellum.Exterior_wmlM2
Right.Cerebellum.White.Matter_volM2	Right.Cerebellum.White.Matter_wmlM2
Left.Cerebellum.White.Matter_volM2	Left.Cerebellum.White.Matter_wmlM2
Right.Hippocampus_volM2	**Right.Hippocampus_wmlM2**
Left.Hippocampus_volM2	**Left.Hippocampus_wmlM2**
Right.Inf.Lat.Vent_volM2	**Right.Inf.Lat.Vent_wmlM2**
Left.Inf.Lat.Vent_volM2	**Left.Inf.Lat.Vent_wmlM2**
Right.Lateral.Ventricle_volM2	**Right.Lateral.Ventricle_wmlM2**
Left.Lateral.Ventricle_volM2	**Left.Lateral.Ventricle_wmlM2**
Right.Pallidum_volM2	Right.Pallidum_wmlM2
Left.Pallidum_volM2	Left.Pallidum_wmlM2
Right.Putamen_volM2	**Right.Putamen_wmlM2**
Left.Putamen_volM2	**Left.Putamen_wmlM2**
Right.Thalamus.Proper_volM2	**Right.Thalamus.Proper_wmlM2**
Left.Thalamus.Proper_volM2	**Left.Thalamus.Proper_wmlM2**
Right.Ventral.DC_volM2	**Right.Ventral.DC_wmlM2**
Left.Ventral.DC_volM2	**Left.Ventral.DC_wmlM2**
Cerebellar.Vermal.Lobules.I-V_volM2	Cerebellar.Vermal.Lobules.I-V_wmlM2
Cerebellar.Vermal.Lobules.VI-VII_volM2	Cerebellar.Vermal.Lobules.VI-VII_wmlM2
Cerebellar.Vermal.Lobules.VIII-X_volM2	Cerebellar.Vermal.Lobules.VIII-X_wmlM2
Left.Basal.Forebrain_volM2	**Left.Basal.Forebrain_wmlM2**
Right.Basal.Forebrain_volM2	Right.Basal.Forebrain_wmlM2
frontal.lobe.WM.right_volM2	**frontal.lobe.WM.right_wmlM2**
frontal.lobe.WM.left_volM2	**frontal.lobe.WM.left_wmlM2**
occipital.lobe.WM.right_volM2	**occipital.lobe.WM.right_wmlM2**
occipital.lobe.WM.left_volM2	**occipital.lobe.WM.left_wmlM2**
parietal.lobe.WM.right_volM2	**parietal.lobe.WM.right_wmlM2**

parietal.lobe.WM.left_volM2	**parietal.lobe.WM.left_wmlM2**
temporal.lobe.WM.right_volM2	**temporal.lobe.WM.right_wmlM2**
temporal.lobe.WM.left_volM2	**temporal.lobe.WM.left_wmlM2**
fornix.right_volM2	**fornix.right_wmlM2**
fornix.left_volM2	**fornix.left_wmlM2**
anterior.limb.of.internal.capsule.right_volM2	**anterior.limb.of.internal.capsule.right_wmlM2**
anterior.limb.of.internal.capsule.left_volM2	**anterior.limb.of.internal.capsule.left_wmlM2**
posterior.limb.of.internal.capsule.inc..cerebral.peduncle.right_volM2	**posterior.limb.of.internal.capsule.inc..cerebral.pedunc**
posterior.limb.of.internal.capsule.inc..cerebral.peduncle.left_volM2	**posterior.limb.of.internal.capsule.inc..cerebral.pedunc**
corpus.callosum_volM2	**corpus.callosum_wmlM2**
Right.ACgG.anterior.cingulate.gyrus_volM2	**Right.ACgG.anterior.cingulate.gyrus_wmlM2**
Left.ACgG.anterior.cingulate.gyrus_volM2	Left.ACgG.anterior.cingulate.gyrus_wmlM2
Right.AIns.anterior.insula_volM2	**Right.AIns.anterior.insula_wmlM2**
Left.AIns.anterior.insula_volM2	Left.AIns.anterior.insula_wmlM2
Right.AOrG.anterior.orbital.gyrus_volM2	**Right.AOrG.anterior.orbital.gyrus_wmlM2**
Left.AOrG.anterior.orbital.gyrus_volM2	Left.AOrG.anterior.orbital.gyrus_wmlM2
Right.AnG.angular.gyrus_volM2	**Right.AnG.angular.gyrus_wmlM2**
Left.AnG.angular.gyrus_volM2	Left.AnG.angular.gyrus_wmlM2
Right.Calc.calcarine.cortex_volM2	**Right.Calc.calcarine.cortex_wmlM2**
Left.Calc.calcarine.cortex_volM2	**Left.Calc.calcarine.cortex_wmlM2**
Right.CO.central.operculum_volM2	Right.CO.central.operculum_wmlM2
Left.CO.central.operculum_volM2	Left.CO.central.operculum_wmlM2
Right.Cun.cuneus_volM2	**Right.Cun.cuneus_wmlM2**
Left.Cun.cuneus_volM2	Left.Cun.cuneus_wmlM2
Right.Ent.entorhinal.area_volM2	Right.Ent.entorhinal.area_wmlM2
Left.Ent.entorhinal.area_volM2	Left.Ent.entorhinal.area_wmlM2
Right.FO.frontal.operculum_volM2	Right.FO.frontal.operculum_wmlM2
Left.FO.frontal.operculum_volM2	Left.FO.frontal.operculum_wmlM2
Right.FRP.frontal.pole_volM2	Right.FRP.frontal.pole_wmlM2
Left.FRP.frontal.pole_volM2	Left.FRP.frontal.pole_wmlM2
Right.FuG.fusiform.gyrus_volM2	Right.FuG.fusiform.gyrus_wmlM2
Left.FuG.fusiform.gyrus_volM2	Left.FuG.fusiform.gyrus_wmlM2
Right.GRe.gyrus.rectus_volM2	Right.GRe.gyrus.rectus_wmlM2
Left.GRe.gyrus.rectus_volM2	Left.GRe.gyrus.rectus_wmlM2
Right.IOG.inferior.occipital.gyrus_volM2	Right.IOG.inferior.occipital.gyrus_wmlM2
Left.IOG.inferior.occipital.gyrus_volM2	Left.IOG.inferior.occipital.gyrus_wmlM2
Right.ITG.inferior.temporal.gyrus_volM2	Right.ITG.inferior.temporal.gyrus_wmlM2
Left.ITG.inferior.temporal.gyrus_volM2	Left.ITG.inferior.temporal.gyrus_wmlM2
Right.LiG.lingual.gyrus_volM2	**Right.LiG.lingual.gyrus_wmlM2**
Left.LiG.lingual.gyrus_volM2	**Left.LiG.lingual.gyrus_wmlM2**
Right.LOrG.lateral.orbital.gyrus_volM2	Right.LOrG.lateral.orbital.gyrus_wmlM2

Left.LOrG.lateral.orbital.gyrus_volM2	Left.LOrG.lateral.orbital.gyrus_wmlM2
Right.MCgG.middle.cingulate.gyrus_volM2	Right.MCgG.middle.cingulate.gyrus_wmlM2
Left.MCgG.middle.cingulate.gyrus_volM2	Left.MCgG.middle.cingulate.gyrus_wmlM2
Right.MFC.medial.frontal.cortex_volM2	**Right.MFC.medial.frontal.cortex_wmlM2**
Left.MFC.medial.frontal.cortex_volM2	Left.MFC.medial.frontal.cortex_wmlM2
Right.MFG.middle.frontal.gyrus_volM2	Right.MFG.middle.frontal.gyrus_wmlM2
Left.MFG.middle.frontal.gyrus_volM2	Left.MFG.middle.frontal.gyrus_wmlM2
Right.MOG.middle.occipital.gyrus_volM2	**Right.MOG.middle.occipital.gyrus_wmlM2**
Left.MOG.middle.occipital.gyrus_volM2	Left.MOG.middle.occipital.gyrus_wmlM2
Right.MOrG.medial.orbital.gyrus_volM2	**Right.MOrG.medial.orbital.gyrus_wmlM2**
Left.MOrG.medial.orbital.gyrus_volM2	Left.MOrG.medial.orbital.gyrus_wmlM2
Right.MPoG.postcentral.gyrus.medial.segment_volM2	Right.MPoG.postcentral.gyrus.medial.segment_wmlM2
Left.MPoG.postcentral.gyrus.medial.segment_volM2	Left.MPoG.postcentral.gyrus.medial.segment_wmlM2
Right.MPrG.precentral.gyrus.medial.segment_volM2	Right.MPrG.precentral.gyrus.medial.segment_wmlM2
Left.MPrG.precentral.gyrus.medial.segment_volM2	Left.MPrG.precentral.gyrus.medial.segment_wmlM2
Right.MSFG.superior.frontal.gyrus.medial.segment_volM2	Right.MSFG.superior.frontal.gyrus.medial.segment_wml
Left.MSFG.superior.frontal.gyrus.medial.segment_volM2	Left.MSFG.superior.frontal.gyrus.medial.segment_wmlM
Right.MTG.middle.temporal.gyrus_volM2	Right.MTG.middle.temporal.gyrus_wmlM2
Left.MTG.middle.temporal.gyrus_volM2	Left.MTG.middle.temporal.gyrus_wmlM2
Right.OCP.occipital.pole_volM2	Right.OCP.occipital.pole_wmlM2
Left.OCP.occipital.pole_volM2	Left.OCP.occipital.pole_wmlM2
Right.OFuG.occipital.fusiform.gyrus_volM2	Right.OFuG.occipital.fusiform.gyrus_wmlM2
Left.OFuG.occipital.fusiform.gyrus_volM2	Left.OFuG.occipital.fusiform.gyrus_wmlM2
Right.OpIFG.opercular.part.of.the.inferior.frontal.gyrus_volM2	Right.OpIFG.opercular.part.of.the.inferior.frontal.gyrus_
Left.OpIFG.opercular.part.of.the.inferior.frontal.gyrus_volM2	Left.OpIFG.opercular.part.of.the.inferior.frontal.gyrus_w
Right.OrIFG.orbital.part.of.the.inferior.frontal.gyrus_volM2	Right.OrIFG.orbital.part.of.the.inferior.frontal.gyrus_wm
Left.OrIFG.orbital.part.of.the.inferior.frontal.gyrus_volM2	Left.OrIFG.orbital.part.of.the.inferior.frontal.gyrus_wml
Right.PCgG.posterior.cingulate.gyrus_volM2	Right.PCgG.posterior.cingulate.gyrus_wmlM2
Left.PCgG.posterior.cingulate.gyrus_volM2	Left.PCgG.posterior.cingulate.gyrus_wmlM2
Right.PCu.precuneus_volM2	**Right.PCu.precuneus_wmlM2**
Left.PCu.precuneus_volM2	Left.PCu.precuneus_wmlM2
Right.PHG.parahippocampal.gyrus_volM2	Right.PHG.parahippocampal.gyrus_wmlM2
Left.PHG.parahippocampal.gyrus_volM2	Left.PHG.parahippocampal.gyrus_wmlM2
Right.PIns.posterior.insula_volM2	Right.PIns.posterior.insula_wmlM2
Left.PIns.posterior.insula_volM2	**Left.PIns.posterior.insula_wmlM2**
Right.PO.parietal.operculum_volM2	**Right.PO.parietal.operculum_wmlM2**
Left.PO.parietal.operculum_volM2	Left.PO.parietal.operculum_wmlM2
Right.PoG.postcentral.gyrus_volM2	**Right.PoG.postcentral.gyrus_wmlM2**
Left.PoG.postcentral.gyrus_volM2	Left.PoG.postcentral.gyrus_wmlM2
Right.POrG.posterior.orbital.gyrus_volM2	Right.POrG.posterior.orbital.gyrus_wmlM2
Left.POrG.posterior.orbital.gyrus_volM2	Left.POrG.posterior.orbital.gyrus_wmlM2

Right.PP.planum.polare_volM2	Right.PP.planum.polare_wmlM2
Left.PP.planum.polare_volM2	Left.PP.planum.polare_wmlM2
Right.PrG.precentral.gyrus_volM2	**Right.PrG.precentral.gyrus_wmlM2**
Left.PrG.precentral.gyrus_volM2	Left.PrG.precentral.gyrus_wmlM2
Right.PT.planum.temporale_volM2	Right.PT.planum.temporale_wmlM2
Left.PT.planum.temporale_volM2	Left.PT.planum.temporale_wmlM2
Right.SCA.subcallosal.area_volM2	Right.SCA.subcallosal.area_wmlM2
Left.SCA.subcallosal.area_volM2	Left.SCA.subcallosal.area_wmlM2
Right.SFG.superior.frontal.gyrus_volM2	Right.SFG.superior.frontal.gyrus_wmlM2
Left.SFG.superior.frontal.gyrus_volM2	**Left.SFG.superior.frontal.gyrus_wmlM2**
Right.SMC.supplementary.motor.cortex_volM2	Right.SMC.supplementary.motor.cortex_wmlM2
Left.SMC.supplementary.motor.cortex_volM2	**Left.SMC.supplementary.motor.cortex_wmlM2**
Right.SMG.supramarginal.gyrus_volM2	**Right.SMG.supramarginal.gyrus_wmlM2**
Left.SMG.supramarginal.gyrus_volM2	Left.SMG.supramarginal.gyrus_wmlM2
Right.SOG.superior.occipital.gyrus_volM2	**Right.SOG.superior.occipital.gyrus_wmlM2**
Left.SOG.superior.occipital.gyrus_volM2	Left.SOG.superior.occipital.gyrus_wmlM2
Right.SPL.superior.parietal.lobule_volM2	Right.SPL.superior.parietal.lobule_wmlM2
Left.SPL.superior.parietal.lobule_volM2	Left.SPL.superior.parietal.lobule_wmlM2
Right.STG.superior.temporal.gyrus_volM2	Right.STG.superior.temporal.gyrus_wmlM2
Left.STG.superior.temporal.gyrus_volM2	Left.STG.superior.temporal.gyrus_wmlM2
Right.TMP.temporal.pole_volM2	Right.TMP.temporal.pole_wmlM2
Left.TMP.temporal.pole_volM2	Left.TMP.temporal.pole_wmlM2
Right.TrIFG.triangular.part.of.the.inferior.frontal.gyrus_volM2	Right.TrIFG.triangular.part.of.the.inferior.frontal.gyrus_v
Left.TrIFG.triangular.part.of.the.inferior.frontal.gyrus_volM2	Left.TrIFG.triangular.part.of.the.inferior.frontal.gyrus_wm
Right.TTG.transverse.temporal.gyrus_volM2	Right.TTG.transverse.temporal.gyrus_wmlM2
Left.TTG.transverse.temporal.gyrus_volM2	Left.TTG.transverse.temporal.gyrus_wmlM2

[a] Note than only 61 ROIs were included in analysis C', given that all others were null for all participants. Those are the bolded and red ROIs for WMLV. Further filtering was made at a level of 5% non-zero or more (n=24). Since all ROIs were included for volumetric ROI-specific analysis (Analysis A"), those are all bolded.

Table S2. Study sample characteristics of eligible study sample by NfL(v1) and NfL(v2) tertiles, overall; HANDLS 2004-2009/2009-2013 (NfL at v_1 and v_2) and HANDLS-SCAN 2011-2015[a]

	NfL at v1			*Nfl at v2*		
	T1	*T2*	*T3*	*T1*	*T2*	*T3*
	(N=60)	*(N=60)*	*(N=59)*	*(N=60)*	*(N=60)*	*(N=59)*
Plasma NfL						
NfL at v_1, Log_e transformed						
Mean±SD	1.49±0.28	1.99±0.11	2.57±0.41***	1.57±0.36	2.087±0.408	2.386±0.450***
IQR	1.37-1.67	1.92-2.09	2.26-2.68	1.37-1.84	1.85-2.24	2.11-2.64
NfL at v_2, Log_e transformed						
Mean±SD	1.81±0.43	2.25±0.54	2.60±0.47***	1.662±0.247	2.168±0.102	2.831±0.498***
IQR	1.57-2.02	1.79-2.37	2.23-2.83	1.47-1.85	2.08-2.25	2.56-2.99
"Tracking high" v_1 through v_2: NfL>8 pg/mL	0.0	18.0	91.0***	0.0	32.0	78.0***
"Tracking low", v_1 through v_2: NfL≤8 pg/mL	80.0	28.0	0.0***	93.0	15.0	0.0***
Socio-demographic factors						
Sex, % males	40.0	48.3	45.8	43.3	41.7	49.2
Age_{v1}	41.9±7.9	47.6±8.4	53.9±6.7***	41.8±7.5	47.6±8.0	54.0±7.4***
Race, % AA	50.0	40.0	33.9	55.0	36.7	32.2*
% above poverty	56.7	66.7	83.1**	60.0	73.3	72.9
Time between v_1 and v_{scan} (days)	2,103±618	1858± 658	1973± 609	1,992±666	1,860±621	2,083± 602
Time between v_2 and v_{scan}(days)	487±471	333±392	413±455	447± 479	334±374	453±465
Imputed covariates, % or Mean±SE						
Body mass index, $kg.m^{-2}$	30.9±0.9	29.4±0.8	27.6±0.7**,[b]	30.0±0.9	29.4±0.8	28.6±0.8
Diabetes						
No	74.7	69.0	72.2	74.0	71.3	69.5
Pre-diabetes	17.0	20.3	15.6	17.3	17.0	18.6
Diabetes	8.3	11.7	12.2	8.7	11.7	11.9
Plasma glucose, mg/dL	97.5± 3.1	99.6±2.6	102.7±4.9	97.1±3.0	97.5± 2.4	105.2±4.9
Creatinine, mg/dL	0.87±0.04	0.89±0.04	0.92±0.04	0.88±0.04	0.86±0.03	0.94±0.02
Urine Specific Gravity	1.019±0.0010	1.020±0.0007	1.018±0.0008	1.0197±0.0010	1.019 ±0.0006	1.019±0.0008
Blood urea nitrogen, mg/dL	12.7±0.5	14.03±0.517	14.56±0.56*	12.50±0.54	13.57±0.40	15.20±0.61***
Alkaline Phosphatase, U/L	70.9±2.4	74.6±3.1	80.2±2.4*	69.3±2.7	73.5±2.2	83.0 ±2.9***,[b]

Uric acid, mg/dL	5.36±0.17	5.79±0.24	5.33 ±0.15 [b]	5.40±0.17	5.44±0.21	5.64±0.18
Albumin, g/dL	4.35±0.04	4.38±0.03	4.30±0.03	4.34±0.04	4.36±0.04	4.32±0.03
Eosinophils, %	2.72±0.22	2.74±0.24	2.78±0.30	2.62±0.23	2.73±0.27	2.89±0.27
25-hydroxyvitamin D, ng/mL	18.5±1.2	22.2±1.5	26.4±1.6***, [b]	18.3±1.3	23.93±1.63	24.81±1.25**
Current drug use, % yes	17.3	17.0	26.1	19.0	23.3	18.0
Self-rated health, %						
Poor/fair	18.3	25.0	22.0	23.3	20.0	22.0
Good	38.3	31.7	40.7	36.7	40.0	33.9
Very good/Excellent	43.4	43.3	37.3	40.0	40.0	44.1
sMRI measures						
Intracranial volume, mm³(mean±SD)	1,327,429±130,020	1,344,990±148,920	1,345,624±148,282	1,333,967±147,315	1,327,240 ±130,181	1,357,026±148,825
Global cortical brain volumes,* mm³ *(mean±SD)						
Total brain volume	1,147,025±107,813	1,144,965±131,262	1,136,569±115,739	1,153,259±123,664	1,132,592± 108,305	1,142,813±122,879
Gray Matter	650,352±61,813	644,497±72,860	632,217±59,947	654,670±67,051	636,968± 62,593	635,484±65,285
White Matter	456,429±47,309	458,894±58,998	456,464±52,520	458805±56111	453,604± 47,453	459,429±55,368
***Regional cortical brain volumes,* mm³ *(mean±SD*)**						
Left Brain						
Frontal GM	95,041±9,466	93,621±10,931	90,943± 9,581*	95,524±9,916	92,329± 10,088	91,765±10,067 *
Frontal WM	85,443±9,303	85,499±11,285	85,030±10,487	85,757±10,817	84,499± 9,541	85,728±10,724
Temporal GM	50,490±5,751	50,786±6,932	49,580±5,690	50,700±6,471	50,225± 5,847	49,936±6,166
Temporal WM	49,119±5,434	49,613±6,900	49,367± 6,015	49,375±6,731	48,983± 5,437	49,747±6,190
Parietal GM	46,756±5,186	46,169± 6,383	45,511± 5,404	47,239±5,675	45,918± 5,437	45,275±5,823
Parietal WM	43,539±4,818	44,201± 6,108	43,953±5,899	43,790±5,723	43,590± 4,932	44,318±6,184
Occipital GM	38,345±4,629	38,574±6,186	37,293±4,690	38,622±5,117	38,286± 5,049	37,304±5,490
Occipital WM	20,893±2,808	21,361±3,143	20,827±2,932	21,123±3,052	21,081± 2,652	20,878±3,190
Right Brain						
Frontal GM	95,162±9,996	93,666±11,204	91,033±9,397*	95,774±10,377	92,076± 10,122	92,029±10,165*
Frontal WM	87,669± 9,819	87,598±11,557	87,386±10,794	88,059±11,292	86,520±9,607	88,086±11,191

Temporal GM	51,615±5,867	51,881±6,486	50,149±5,577	51,823±6,186	51,021± 5,952	50,811±5,928
Temporal WM	49,825±5,473	50,195±6,841	49,716±5,855	50,123±6,468	49,504± 5,555	50,114± 6,187
Parietal GM	47,582±5,241	46,855±6,437	45,866±5,471	48,027±5,569	46,319± 5,383	45,958±6,164*
Parietal WM	41,351±4,709	41,924±5,982	41,779 ±5,665	41,620±5,545	41,468±4,900	41,968±5,949
Occipital GM	39038±4,898	39,733±6,087	39,233±5,215	39,541±5,470	39,529± 5,313	38,929±5,492
Occipital WM	20,441±2,768	21,016±3,042	20,993±2,990	20,692±3,029	20,762± 2,842	20996±2959
Hippocampal volume, mm^3						
Hippocampus, Left	3,559±391	3,553±400	3,499±368	3,543±416	3,603±345	3,464±386*
Hippocampus, Right	3,850±424	3,836±439	3,797±380	3,847±460	3,841±364	3,794±415
Hippocampus, Left, as % TBV	0.269±0.022	0.265±0.026	0.261±0.024	0.266±0.019	0.273±0.023	0.256±0.027
Hippocampus, Right, as % TBV	0.291±0.024	0.286±0.025	0.284±0.024	0.290±0.021	0.290± 0.026	0.281±0.026
White matter lesion volume, mm^3, Log_e transformed	4.325±6.254	6.129±1.143	6.505±1.161**[,b]	4.689±5.451	6.249± 1.275	6.013±3.452
White matter lesion volume, mm^3, % TBV, Log_e transformed	-5.164±6.243	-3.372±1.148	-2.996±1.152**[,b]	-4.804±5.433	-3.240± 1.254	-3.497±3.464

Abbreviations: Age_{v1}=age measured at HANDLS visit 1 (2004-2009); CV=Coefficient of Variation; IQR=Interquartile Range; GM=Gray Matter; HANDLS=Healthy Aging in Neighborhoods of Diversity Across the Life Span; HANDLS-SCAN=Brain magnetic resonance imaging scan ancillary study of HANDLS; IQR=Interquartile range (25^{th}-75^{th} percentile); NfL=Neurofilament Light; sMRI=Structural Magnetic Resonance Imaging; T1-T3=tertiles; v_1=visit 1 of HANDLS (2004-2009); v2=visit 2 of HANDLS (2009-2013); v_{scan}=HANDLS-SCAN visit (2011-2015); WM=White Matter.

[a] Values are Mean±SD (Mean±SE for imputed covariates), or %. Volumes are expressed in mm^3.

[b] P<0.05 after further adjustment for age, sex, race, poverty status for socio-demographic and sMRI measures.

*P<0.05 **P<0.010 ***P<0.001 for null hypothesis of no trend across tertiles of NfL, Log_e transformed, tertiles.

Table S3. Selected covariate-adjusted associations from analyses A (global GM and WM volumes), A' (regional cortical GM/WM), B (hippocampal volume) and C (White matter lesion volume) vs. visit 1 NfL (overall and stratified by sex): ordinary least square analyses; HANDLS 2004-2009 and HANDLS-SCAN 2011-2015: Sensitivity analyses[a]

	Model 3		*Model 4*		*Model 5*		*Model 6*	
Total sample (N=179)	*β3*	*(SE3)*	*β4*	*(SE4)*	*β5*	*(SE5)*	*β6*	*(SE6)*
sMRI, Analysis A								
Total brain	+298	(17,228)	-4,752	(16,520)	-2,779	(17,177)	+8,533	(17,078)
GM	-5,805	(9,203)	-7,780	(8,952)	-4,429	(9,214)	+1,544	(9,106)
WM	+2,738	(8,400)	+561	(8,038)	+44	(8,336)	+3,722	(8,345)
sMRI, Analysis B								
Hippocampus, Left	-56.4	(56.3)	-46.1	(56.0)	-30.3	(56.3)	-46.8	(56.3)
Hippocampus, Right	-52.3	(57.8)	-47.1	(57.6)	-9.7	(58.1)	-36.3	(58.1)
Analysis C								
White matter lesion volume, Log_e transformed	**+2.508**	**(0.712)[e, f]**	**+2.347**	**(0.708)[e, f]**	**+2.56**	**(0.71)[e,f]**	**+2.300**	**(0.712)[e,f]**
Males (N=80)								
sMRI, Analysis A								
Total brain	-5,017	(26,145)	-20,634	(26,292)	-11,789	(26,211)	-6,189	(26,185)
GM	-10,677	(13,628)	-19,117	(13,669)	-10,592	(13,605)	-7,201	(13,546)
WM	-1,054	(12,708)	-5,860	(12,804)	-5,827	(12,745)	-4,182	(12,735)
sMRI, Analysis B								
Hippocampus, Left	-106.6	(80.7)	-86.6	(86.0)	-104.7	(81.6)	-30.5	(78.8)
Hippocampus, Right	-86.0	(81.1)	-93.5	(85.7)	-66.1	(83.3)	-2.5	(81.3)
Analysis C								
White matter lesion volume, Log_e transformed	**+1.58**	**(0.76)[d]**	**+1.94**	**(0.77)[d]**	+1.41	(0.76)[c]	+1.36	(0.76)[c]
Females (N=99)								
sMRI, Analysis A								

Total brain	12,621	(23,535)	+21,124	(21,927)	+17,345	(23,864)	+34,749	(22,913)
GM	4,233	(13,000)	+9,706	(12,492)	+8,932	(13,210)	+17,400	(12,794)
WM	11,325	(11,481)	+13,332	(10,532)	+11,997	(11,524)	+18,537	(11,155)
sMRI, Analysis B								
Hippocampus, Left	+56.1	(78.9)	+70.1	(78.3)	+110.7	(79.1)	+29.0	(79.1)
Hippocampus, Right	18.3	(86.1)	+25.4	(85.6)	+70.6	(85.4)	-25.2	(85.4)
Analysis C								
White matter lesion volume, Log_e transformed	**+4.33**	**(1.27)** [e]	**+3.96**	**(1.25)** [e]	**+4.47**	**(1.27)**[e]	**+3.76**	**(1.30)** [e]

Abbreviations: Age_{v1}=age measured at HANDLS visit 1 (2004-2009); GM=Gray Matter; HANDLS=Healthy Aging in Neighborhoods of Diversity Across the Life Span; HANDLS-SCAN=Brain magnetic resonance imaging scan ancillary study of HANDLS; NfL=Neurofilament Light Chain; SE=Standard Error; sMRI=Structural Magnetic Resonance Imaging; v_1=visit 1 of HANDLS (2004-2009); v2=visit 2 of HANDLS (2009-2013); v_{scan}=HANDLS-SCAN visit (2011-2015); WM=White Matter

[a] Values are adjusted linear regression coefficients β with associated SE. (N) is the sample size in each analysis. Model 2 in Table 2 was adjusted for Age_{v1}, sex, race, poverty status and time of follow-up between visit 1 and v_{scan} and BMI. Volumes are expressed in mm^3.

[b] Model 3 is a sensitivity analysis further adjusting Model 2 (Table 2) for Diabetes and serum glucose levels; Model 4 is a sensitivity analysis further adjusting Model 2 (Table 2) for selected markers of kidney and liver disease (creatinine, urinary specific gravity, blood urea nitrogen, alkaline phosphatase and uric acid); Model 5 is a sensitivity analysis further adjusting Model 2 (Table 2) for selected inflammatory factors (25-hydroxyvitamin D, serum albumin, eosinophils as % of total white blood cells); Model 6 is a sensitivity analysis further adjusting Model 2 (Table 2) for other lifestyle and health-related covariates (current drug use, self-rated health).

[c] $P<0.10$ [d] $P<0.05$ [e] $P<0.010$ for null hypothesis that exposure main effect is =0 in each model, stratified or unstratified.

[f] $P<0.10$ for null hypothesis that exposure×sex 2-way interaction term is =0 in the unstratified model with exposure and sex included as main effects.

Table S4. Selected covariate-adjusted associations from analyses A (global GM and WM volumes), A' (regional cortical GM/WM), B (hippocampal volume) and C (White matter lesion volume) vs. Visit 2 NfL (overall and stratified by sex): ordinary least square analyses; HANDLS 2009-2013 and HANDLS-SCAN 2011-2015: Sensitivity analyses[a]

	Model 3		*Model 4*		*Model 5*		*Model 6*	
Total sample (N=179)	*β3*	*(SE3)*	*β4*	*(SE4)*	*β5*	*(SE5)*	*β6*	*(SE6)*
sMRI, Analysis A								
Total brain	-4,558	(13,860)	-1,262	(13,622)	-3,969	(13,432)	-2,387	(13,314)
GM	-6,720	(7,397)	-6,186	(7,393)	-5,269	(7,208)	-4,339	(7,069)
WM	-1,416	(6.759)	+898	(6,637)	-1,682	(6,514)	-964	(6,505)
sMRI, Analysis B								
Hippocampus, Left	**-140.1**	**(44.1)[e]**	**-137.6**	**(45.3)[e]**	**-125.3**	**(42.9)[e]**	**-123.0**	**(42.9)[e]**
Hippocampus, Right	**-118.5**	**(45.7)[e]**	**-122.6**	**(46.8)[e]**	**-96.1**	**(44.9)[d]**	**-97.9**	**(44.7)[d]**
Analysis C								
White matter lesion volume, Log_e transformed	+0.48	(0.60)[f]	+0.38	(0.60)[f]	+0.47	(0.58)[f]	+0.471	(0.571)[f]
Males (N=80)								
sMRI, Analysis A								
Total brain	-15,062	(21,889)	-22,004	(21,340)	-17,661	(21,169)	-14,744	(21,431)
GM	-11,374	(11,421)	-15,548	(11,136)	-12,155	(11,005)	-9,783	(11,094)
WM	-7,185	(10,631)	-9,501	(10,398)	-8,266	(10,267)	-7,348	(10,396)
sMRI, Analysis B								
Hippocampus, Left	**-169.1**	**(65.6)[d]**	**-159.3**	**(68.1)[d]**	**-154.5**	**(64.4)[d]**	**-139.5**	**(62.1)[d]**
Hippocampus, Right	**-158.9**	**(66.0)[d]**	**-155.9**	**(68.1)[d]**	-123.4	(66.5)[c]	-127.6	(64.3)[c]
Analysis C								
White matter lesion volume, Log_e transformed	-0.274	(0.655)	-0.048	(0.660)	-0.270	(0.636)	-0.286	(0.637)
Females (N=99)								
sMRI, Analysis A								

Total brain	+7,701	(19,505)	+28,117	(19,772)	+11,430	(19,285)	14,539	(18,640)
GM	-2,561	(10,769)	+5,620	(11,313)	+888	(10,709)	2,346	(10,399)
WM	+8,453	(9,518)	+18,417	(9,472)[c]	+8,872	(9,319)	10,012	(9,076)
sMRI, Analysis B								
Hippocampus, Left	-40.9	(65.5)	-34.7	(71.9)	-17.9	(64.9)	-34.5	(63.2)
Hippocampus, Right	-29.6	(71.5)	-36.7	(78.3)	-11.1	(69.7)	-31.5	(68.3)
Analysis C								
White matter lesion volume, Log_e transformed	+1.68	(1.11)[f]	+1.39	(1.20)[f]	+1.63	(1.09)	+1.42	(1.08)

Abbreviations: Age_{v1}=age measured at HANDLS visit 1 (2004-2009); GM=Gray Matter; HANDLS=Healthy Aging in Neighborhoods of Diversity Across the Life Span; HANDLS-SCAN=Brain magnetic resonance imaging scan ancillary study of HANDLS; NfL=Neurofilament Light Chain; SE=Standard Error; sMRI=Structural Magnetic Resonance Imaging; v_1=visit 1 of HANDLS (2004-2009); v2=visit 2 of HANDLS (2009-2013); v_{scan}=HANDLS-SCAN visit (2011-2015); WM=White Matter.

[a] Values are adjusted linear regression coefficients β with associated SE. (N) is the sample size in each analysis. Model 2 in Table 3 was adjusted for Age_{v1}, sex, race, poverty status, intra-cranial volume for analyses B and C, and time of follow-up between visit 1 and v_{scan} and BMI. Volumes are expressed in mm^3.

[b] Model 3 is a sensitivity analysis further adjusting Model 2 (Table 3) for Diabetes and serum glucose levels; Model 4 is a sensitivity analysis further adjusting Model 2 (Table 3) for selected markers of kidney and liver disease (creatinine, urinary specific gravity, blood urea nitrogen, alkaline phosphatase and uric acid); Model 5 is a sensitivity analysis further adjusting Model 2 (Table 3) for selected inflammatory factors (25-hydroxyvitamin D, serum albumin, eosinophils as % of total white blood cells); Model 6 is a sensitivity analysis further adjusting Model 2 (Table 3) for other lifestyle and health-related covariates (current drug use, self-rated health).

[c] $P<0.10$ [d] $P<0.05$ [e] $P<0.010$ for null hypothesis that exposure main effect is =0 in each model, stratified or unstratified.

[f] $P<0.10$ for null hypothesis that exposure×sex 2-way interaction term is =0 in the unstratified model with exposure and sex included as main effects.

Table S5. Summary of findings from sensitivity analyses with NfL at v_1 and at v_2 (for hippocampal and lesion volume outcomes), adjusted for intracranial volume, by race HANDLS-SCAN 2011-2015

	NfL at v_1					
	Model 1	Model 2	Model 3	Model 4	Model 5	Model 6
	African Americans (n=74)					
Hippocampus, Left	-6.36±73.59 P=0.93	-38.00±85.82 P=0.66	-62.2±87.7 P=0.48	-32.4±94.7 P=0.73	-40.10±89.2 P=0.66	-15.31±87.36 P=0.86
Hippocampus, Right	+6.77±72.09 P=0.93	-40.77±83.6 P=0.63	-48.7±81.7 P=0.55	-45.4±90.8 P=0.62	-32.8±86.7 P=0.71	-13.25±85.48 P=0.88
Lesion volume, Log_e transformed	+1.61±0.84 P=0.061	**+2.36±0.97** **P=0.018**	**+2.37±1.04** **P=0.026**	**+2.28±1.03** **P=0.031**	**+2.37±1.02** **P=0.023**	+1.98±1.00 P=0.052
	Whites (n=105)					
Hippocampus, Left	-103.6±75.1 P=0.17	-94.0±74.7 P=0.21	-111.7±81.6 P=0.17	-106.0±78.0 P=0.18	-89.2±79.8 P=0.27	-107.0±78.2 P=0.18
Hippocampus, Right	-116.7±77.7 P=0.14	-103.5±76.6 P=0.18	-128.7±83.6 P=0.13	-127.3±80.0 P=0.12	-94.2±81.8 P=0.25	-124.3±80.0 P=0.12
Lesion volume, Log_e transformed	**+2.66±1.00** **P=0.009**	**+2.71±1.01** **P=0.008**	**+3.09±1.10** **P=0.006**	**+2.76±1.05** **P=0.010**	**+3.24±1.06** **P=0.003**	**+2.85±1.05** **P=0.008**
	NfL at v_2					
	Model 1	Model 2	Model 3	Model 4	Model 5	Model 6
	African Americans (n=74)					
Hippocampus, Left	-95.04±53.00 P=0.077	-103.2±53.8 P=0.060	**-136.6±54.3** **P=0.015**	-116.0±58.6 P=0.053	**-115.6±54.6** **P=0.038**	-104.3±52.8 P=0.053
Hippocampus, Right	-67.50±52.51	-78.7±53.0	**-107.2±50.6**	-99.3±57.2	-84.0±54.0	-78.5±52.3

	P=0.20	P=0.14	**P=0.038**	P=0.088	P=0.13	P=0.14
Lesion volume, Log_e transformed	+0.201±0.639 P=0.75	+0.241±0.652 P=0.71	+0.165±0.686 P=0.81	+0.259±0.702 P=0.71	+0.232±0.672 P=0.73	+0.174±0.641 P=0.79
	Whites (n=105)					
Hippocampus, Left	**-164.9±67.0** **P=0.016**	**-158.2±66.6** **P=0.020**	**-177.9±70.8** **P=0.014**	**-183.3±71.0** **P=0.011**	**-158.2±67.3** **P=0.021**	**-157.5±67.1** **P=0.021**
Hippocampus, Right	**-153.0±70.0** **P=0.031**	**-143.6±68.7** **P=0.039**	**-166.1±73.1** **P=0.025**	**-180.0±73.6** **P=0.017**	**-141.2±69.7** **P=0.046**	**-144.0±69.4** **P=0.041**
Lesion volume, Log_e transformed	+0.830±0.939 P=0.38	+0.853±0.945 P=0.37	+0.889±1.010 P=0.38	+0.622±1.011 P=0.54	+0.871±0.954 P=0.36	+0.838±0.951 P=0.38

Abbreviations: Age_{v1}=age measured at HANDLS visit 1 (2004-2009); HANDLS=Healthy Aging in Neighborhoods of Diversity Across the Life Span; HANDLS-SCAN=Brain magnetic resonance imaging scan ancillary study of HANDLS; NfL=Neurofilament Light; SE=Standard Error; v_1=visit 1 of HANDLS (2004-2009); v2=visit 2 of HANDLS (2009-2013); v_{scan}=HANDLS-SCAN visit (2011-2015).

[a] Values are adjusted linear regression coefficients β with associated SE. (N) is the sample size in each analysis. Volumes are expressed in mm^3.

[b] Model 1 adjusted for Age_{v1}, sex, poverty status, length of follow-up between v_1 and v_{scan} and intracranial volume (ICV). Model 2 is Model 1 further adjusted for BMI. Model 3 is a sensitivity analysis further adjusting Model 2 for Diabetes and serum glucose levels; Model 4 is a sensitivity analysis further adjusting Model 2 for selected markers of kidney and liver disease (creatinine, urinary specific gravity, blood urea nitrogen, alkaline phosphatase and uric acid); Model 5 is a sensitivity analysis further adjusting Model 2 for selected inflammatory factors (25-hydroxyvitamin D, serum albumin, eosinophils as % of total white blood cells); Model 6 is a sensitivity analysis further adjusting Model 2 for other lifestyle and health-related covariates (current drug use, self-rated health).

[c] P<0.10 for null hypothesis that exposure×race 2-way interaction term is =0 in the unstratified model with exposure and race included as main effects.

Table S6. Summary of findings from sensitivity analyses with NfL at v_1 and v_2 (for total brain, Gray Matter and White Matter volumes), by race HANDLS-SCAN 2011-2015

	NfL at v_1					
	Model 1	Model 2	Model 3	Model 4	Model 5	Model 6
	African Americans (n=74)					
Total brain	-42,535±23,258 [c] P=0.072	-47,311±27,615 [c] P=0.091	**-62,323±28,271** [c] **P=0.031**	-56,097±28,427 [c] P=0.053	-51,588±28,475 [c] P=0.075	-40,957±28,791 [c] P=0.16
Gray matter	-25,503±13,247 [c] P=0.058	-27,733±15,733 [c] P=0.083	**-38,762±15,912** [c] **P=0.018**	-32,888±16,461 [c] P=0.050	-28,055±16,300 [c] P=0.090	-20,177±16,183 [c] P=0.22
White matter	15,747±10,775 [c] P=0.15	-19,734±12,770 [c] P=0.13	-24,110±13,285 [c] P=0.074	-23,458±13,059 [c] P=0.078	-23,158±13,112 [c] P=0.082	-20,743±13,336 [c] P=0.13
	Whites (n=105)					
Total brain	+30,270±21,336 P=0.16	+31,171±21,488 P=0.15	+38,651±23,192 P=0.099	+21,520±21,772 P=0.33	+28,970±22,940 P=0.21	+36,303±22,273 P=0.11
Gray matter	+8,545±11,013 P=0.44	+9,370±11,060 P=0.40	+11,453±11,994 P=0.34	+4,643±11,362 P=0.68	+10,039±11,861 P=0.40	12,252±11,474 P=0.29
White matter	+16,599±10,783 P=0.13	16,860±10,869 P=0.12	+20,509±11,772 P=0.085	+12,833±11,032 P=0.25	+15,429±11,564 P=0.19	18,170±11,253 P=0.11
	NfL at v_2					
	Model 1	Model 2	Model 3	Model 4	Model 5	Model 6
	African Americans (n=74)					
Total brain	-18,548±17,918 P=0.30	-16,876±18,332 P=0.36	-26,585±18,846 P=0.16	-19,517±19,497 P=0.32	-20,992±18,608 P=0.26	-15,248±18,375 P=0.41

Gray matter	-10,746±10,229 P=0.30	-9,607±10,457 P=0.36	-16,393±10,558 P=0.13	+2,275±10,387 P=0.83	-11,545±10,665 P=0.28	-8,370±10,289 P=0.42
White matter	-8,375±8,232 P=0.31	-8,244±8,437 P=0.33	-11,337±8,815 P=0.20	+8,055±9,475 P=0.40	-10,227±8,529 P=0.24	-7,864±8,507 P=0.36
	Whites (n=105)					
Total brain	+11,911±19,691 P=0.55	+12,468±19,814 P=0.53	+15,833±20,980 P=0.45	+15,111±20,373 P=0.46	+11,458±20,030 P=0.57	+12,756±19,958 P=0.52
Gray matter	-383.7±10,112 P=0.97	+172±10,148 P=0.99	+667±10,780 P=0.95	-300±10,625 P=0.98	+27±10,325 P=1.00	+278±10,220 P=0.98
White matter	+7,226±9,961 P=0.47	+7,365±10,031 P=0.47	+8,928±10,657 P=0.40	+9,793±10,321 P=0.35	+6,683±10,101 P=0.51	+7,565±10,074 P=0.46

Abbreviations: Age_{v1}=age measured at HANDLS visit 1 (2004-2009); HANDLS=Healthy Aging in Neighborhoods of Diversity Across the Life Span; HANDLS-SCAN=Brain magnetic resonance imaging scan ancillary study of HANDLS; NfL=Neurofilament Light; SE=Standard Error; sMRI=Structural Magnetic Resonance Imaging; v_1=visit 1 of HANDLS (2004-2009); v2=visit 2 of HANDLS (2009-2013); v_{scan}=HANDLS-SCAN visit (2011-2015).

[a] Values are adjusted linear regression coefficients β with associated SE. (N) is the sample size in each analysis. Volumes are expressed in mm^3.

[b] Model 1 adjusted for Age_{v1}, sex, poverty status and length of follow-up between v_1 and v_{scan}. Model 2 is Model 1 further adjusted for BMI. Model 3 is a sensitivity analysis further adjusting Model 2 for Diabetes and serum glucose levels; Model 4 is a sensitivity analysis further adjusting Model 2 for selected markers of kidney and liver disease (creatinine, urinary specific gravity, blood urea nitrogen, alkaline phosphatase and uric acid); Model 5 is a sensitivity analysis further adjusting Model 2 for selected inflammatory factors (25-hydroxyvitamin D, serum albumin, eosinophils as % of total white blood cells); Model 6 is a sensitivity analysis further adjusting Model 2 for other lifestyle and health-related covariates (current drug use, self-rated health).

[c] $P<0.10$ for null hypothesis that exposure×race 2-way interaction term is =0 in the unstratified model with exposure and race included as main effects.

Table S7. Tracking high and Tracking low NfL exposures vs. Left/Right hippocampal volumes and WMLV, overall and by sex

	Tracking high NfL exposure					
	Model 1	Model 2	Model 3	Model 4	Model 5	Model 6
	Overall (n=179)					
Hippocampus, Left	**-137.94 ±50.51** **P=0.007**	**-134.84±52.12** **P=0.011**	**-139.99±52.56** **P=0.009**	**-135.47±53.97** **P=0.013**	**-130.64±54.23** **P=0.017**	**-136.16±52.68** **P=0.011**
Hippocampus, Right	**-134.12 ± 52.26** **P=0.011**	**-130.12±53.93** **P=0.017**	**-136.70±54.05** **P=0.012**	**-140.09±55.42** **P=0.012**	**-120.53±55.81** **P=0.032**	**-131.11±54.40** **P=0.017**
Lesion volume, Log_e transformed	+1.01±0.67 P=0.13	+1.13±0.69 P=0.10	+1.10±0.70 P=0.12	+1.18±0.71 P=0.098	+1.16 ± 0.71 P=0.11	+1.06±0.69 P=0.13
	Males (n=80)					
Hippocampus, Left	**-194.31±78.53** **P=0.016**	**-188.04 ±80.24** **P=0.022**	**-198.11±81.67** **P=0.018**	**-209.90± 90.55** **P=0.024**	**-207.88± 85.62** **P=0.018**	-143.60± 80.96 P=0.081
Hippocampus, Right	**-191.19± 80.71** **P=0.020**	**-175.27±81.80** **P=0.036**	**-195.03±81.85** **P=0.020**	**-230.25±89.66** **P=0.013**	**-191.28±86.01** **P=0.030**	-139.94± 83.30 P=0.098
Lesion volume, Log_e transformed	+1.32 ± 0.76 P=0.087	+1.26±0.78 P=0.11	+1.29±0.80 P=0.11	+1.77±0.85 P=0.042	+1.18±0.82 P=0.15	+1.16±0.81 P=0.16
	Females (n=99)					
Hippocampus, Left	-45.22± 64.86 P=0.49	-39.89 ± 67.57 P=0.56	-47.73±67.12 P=0.48	-29.54± 71.32 P=0.68	-21.03±70.02 P=0.77	-36.94± 66.36 P=0.58
Hippocampus, Right	-45.06±69.71 P=0.52	-46.81± 72.66 P=0.52	-51.61±73.14 P=0.48	-47.09±77.66 P=0.55	-27.25±74.99 P=0.72	-44.59±71.58 P=0.54
Lesion volume, Log_e transformed	+0.67±1.09 P=0.54	+1.05± 1.13 P=0.35	+1.03± 1.14 P=0.37	+1.05±1.20 P=0.38	+1.21± 1.18 P=0.31	+1.06 ±1.14 P=0.35

	Tracking low NfL exposure					
	Model 1	Model 2	Model 3	Model 4	Model 5	Model 6
	Overall (n=179)					
Hippocampus, Left	-14.25± 50.40 P=0.91	-19.64±50.77 P=0.70	-18.15±50.99 P=0.72	-20.92±52.54 P=0.69	-25.96±51.66 P=0.62	-20.04± 51.06 P=0.70
Hippocampus, Right	21.41± 52.01 [c] P=0.68	16.20±52.41 [c] P=0.76	+18.74 ±52.34 [c] P=0.72	+28.54 ±53.91 [c] P=0.60	+5.48± 53.53 [c] P=0.92	+15.85±52.61 [c] P=0.76
Lesion volume, Log_e transformed	-1.20±0.65 [c] P=0.066	-1.25±0.66 [c] P=0.059	-1.23±0.66 [c] P=0.063	-1.22 ±0.68 [c] P=0.074	-1.25±0.67 [c] P=0.064	-1.21± 0.66 [c] P=0.068
	Males (n=80)					
Hippocampus, Left	62.36±81.39 P=0.45	70.01±81.89 P=0.40	77.22± 82.55 P=0.35	66.30 ±88.03 P=0.45	85.21±85.52 P=0.32	57.80±79.26 P=0.47
Hippocampus, Right	137.71±82.14 P=0.10	151.44± 81.58 P=0.068	**164.39± 80.82** **P=0.046**	+164.58±85.92 P=0.060	+153.95±85.24 P=0.075	140.09±79.96 P=0.084
Lesion volume, Log_e transformed	-0.390±0.773 P=0.62	-0.448±0.779 P=0.57	-0.472±0.792 P=0.55	-0.626±0.818 P=0.45	-0.300±0.812 P=0.71	-0.407± 0.787 P=0.61
	Females (n=99)					
Hippocampus, Left	-92.34±59.78 P=0.13	-104.87±61.59 P=0.092	-92.83±61.79 P=0.14	-106.55± 65.21 P=0.11	-120.66±62.09 P=0.055	-89.18± 60.43 P=0.14
Hippocampus, Right	-86.723 64.42658± P=0.18	-93.14±66.59 P=0.17	-86.37±67.55 P=0.20	-95.72± 71.28 P=0.18	-112.81±67.06 P=0.096	-76.80±65.53 P=0.24
Lesion volume, Log_e transformed	-1.82 ±1.00 P=0.073	**-2.20 ±1.02** **P=0.035**	**-2.19 ±1.04** **P=0.039**	-1.90 ±1.09 P=0.086	**-2.33±1.05** **P=0.029**	-2.04 ±1.03 P=0.050

Abbreviations: Age_{v1}=age measured at HANDLS visit 1 (2004-2009); HANDLS=Healthy Aging in Neighborhoods of Diversity Across the Life Span; HANDLS-SCAN=Brain magnetic resonance imaging scan ancillary study of HANDLS; NfL=Neurofilament Light; SE=Standard Error; sMRI=Structural Magnetic Resonance Imaging; v_1=visit 1 of HANDLS (2004-2009); v2=visit 2 of HANDLS (2009-2013); v_{scan}=HANDLS-SCAN visit (2011-2015).

[a] Values are adjusted linear regression coefficients β with associated SE. (N) is the sample size in each analysis. Volumes are expressed in mm^3.

[b] Model 1 adjusted for Age_{v1}, sex, poverty status and length of follow-up between v_1 and v_{scan} and intracranial volume (ICV). Model 2 is Model 1 further adjusted for BMI. Model 3 is a sensitivity analysis further adjusting Model 2 for Diabetes and serum glucose levels; Model 4 is a sensitivity analysis further adjusting Model 2 for selected markers of kidney and liver disease (creatinine, urinary specific gravity, blood urea nitrogen, alkaline phosphatase and uric acid); Model 5 is a sensitivity analysis further adjusting Model 2 for selected inflammatory factors (25-hydroxyvitamin D, serum albumin, eosinophils as % of total white blood cells); Model 6 is a sensitivity analysis further adjusting Model 2 for other lifestyle and health-related covariates (current drug use, self-rated health).

[c] $P<0.10$ for null hypothesis that exposure×race 2-way interaction term is =0 in the unstratified model with exposure and race included as main effects.

Table S8. Ranking of top ROI-specific WMLV associated with NfL at v1, overall, with p<0.05: cubic root transformed WMLV

OUTCOME	idnum	EXPOSURE	Effect size	stderr	dof	t	p
zLPLIC_rightw	20	zLnNFLw1	0.383136	0.089379	171	4.286642	3.02E-05
zLfrontal_lobe_WM_right_wml	9	zLnNFLw1	0.264219	0.086229	171	3.064167	0.002537
zLfrontal_lobe_WM_left_wml	10	zLnNFLw1	0.238184	0.086363	171	2.75795	0.006449
zLRight_Lateral_Ventricle_wml	5	zLnNFLw1	0.242187	0.090636	171	2.6721	0.008267
zLLeft_Lateral_Ventricle_wml	6	zLnNFLw1	0.232254	0.090852	171	2.556383	0.011447
zLparietal_lobe_WM_right_wml	13	zLnNFLw1	0.22816	0.090593	171	2.518516	0.012703
zLRight_Caudate_wml	1	zLnNFLw1	0.223711	0.092048	171	2.430366	0.016117
zLcorpus_callosum_wml	22	zLnNFLw1	0.206543	0.092932	171	2.222516	0.02756
zLALIC_rightw	18	zLnNFLw1	0.193063	0.091697	171	2.105436	0.036714

[a] Note than only 24 ROIs were included in analysis C', given that all others were null or with <5% non-zero volume.